

Sensitivity of seismic velocity changes to the tidal strain at different lapse-times: Data analyses of a small seismic array at Izu-Oshima volcano

Tomoya Takano¹, Takeshi Nishimura¹, Hisashi Nakahara¹, Hideki Ueda², Eisuke Fujita²

¹Department of Geophysics, Graduate School of Science, Tohoku University, Sendai, Japan

²National Research Institute for Earth Science and Disaster Prevention, Tsukuba, Japan

Key Points:

- Seismic velocity decreases and increases during dilatation and contraction periods, respectively, at lapse-times from 2 to 7 s.
- Array analysis enables us to understand wave properties of cross-correlations functions accurately.
- Strain sensitivity of seismic velocity changes decreases with lapse-times because scattered body waves contaminate the cross correlation functions.

This article has been accepted for publication and undergone full peer review but has not been through the copyediting, typesetting, pagination and proofreading process which may lead to differences between this version and the Version of Record. Please cite this article as doi: 10.1029/2018JB016235

Corresponding author: Tomoya Takano, tomoya.takano.p6@dc.tohoku.ac.jp

Abstract

We investigate seismic velocity changes in response to the tidal strain at Izu-Oshima volcano, Japan, by analyzing the data of permanent seismic stations and a small seismic array to evaluate the characteristics of strain sensitivity of velocity changes. We estimate the seismic velocity changes by phase differences between cross-correlations functions of ambient noises at the frequency of 2–4 Hz stacked for time periods with different tidal strain amplitudes. The seismic velocity changes decrease and increase during dilatation and contraction periods, respectively, when analyzing the cross-correlations functions at early lapse-times ranging from 2 to 7 s. The strain sensitivity of seismic velocity changes is estimated to be $(-2.1 \pm 0.2) \times 10^4$ at the early lapse-times. However, we find that strain sensitivity of the seismic velocity changes decreases when analyzing the cross-correlation functions at later lapse-times from 7 s to 35 s. Applying an array analysis to the cross-correlation functions, we observe apparent velocities of about 1 km/s at the early lapse-times and those of higher than 1 km/s at the late lapse-times. Since the group velocity of Rayleigh waves is 1.1 km/s at Izu-Oshima volcano, the apparent velocities at the late lapse-times may indicate the scattered or reflected body waves incident from a deeper region. Decrease of strain sensitivity with the lapse times therefore results from the emergence of body waves on the late lapse-times. These results highlight the need to pay attention to wave types of cross correlation functions and their paths to interpret seismic velocity changes.

1 Introduction

Seismic velocity changes caused by seismic and volcanic activities provide us information about elastic perturbations of the shallow structure. Multiply scattered waves (coda waves) have a high sensitivity to tiny structural changes because the coda waves sample the media multiple times [Snieder *et al.*, 2002]. For example, Poupinet *et al.* [1984] detected seismic velocity reductions of about 1% around the hypocentral area of the Coyote Lake earthquake (M_L 5.9) within the coda of repeating earthquakes. Nishimura *et al.* [2005] examined temporal changes of the crust around Iwate volcano through repeated active seismic experiments, and detected that the seismic velocity decreased down to about 1% during the occurrence of a M 6.1 earthquake. However, these seismic sources are sparse in time and space. It has been demonstrated that cross-correlation functions (CCFs) of diffuse wave fields converge to Green's functions between two receivers [Weaver and

46 *Lobkis, 2001; Snieder, 2004]. The coda part of the CCF is composed of the multiply scat-*
47 *tered waves. The consequence is that CCFs of ambient noise have been successfully ap-*
48 *plied to detect seismic velocity changes caused by large earthquakes around fault zones*
49 *[e.g. Brenguier et al., 2008] or in subduction zones [Rivet et al., 2011], inflations of vol-*
50 *canic edifices before eruption [e.g. Nagaoka et al., 2010], and water level variations due to*
51 *precipitation [e.g. Sens-Schönfelder and Wegler, 2006].*

52 On the other hand, the physical mechanism of seismic velocity changes is still un-

53 der debate. Strong ground motion reduces seismic velocities by the reduction of rigidity at

54 the near-surface [Rubinstein and Beroza, 2005; Sawazaki et al., 2006; Peng and Ben-Zion,

55 2006]. Such seismic velocity reductions are expected to be shallow and to correlate with

56 the strength of shaking, which is clarified by analyzing seismic data recorded at the top

57 and bottom of a borehole [Sawazaki et al., 2009; Takagi et al., 2012; Nakata and Snieder,

58 2012]. Water level variation due to precipitation leads to pore pressure changes, and seis-

59 mic velocity changes thereby are also sensitive to precipitation [Sens-Schönfelder and We-

60 gler, 2006; Meier et al., 2010; Rivet et al., 2015; Wang et al., 2017]. Strain changes cause

61 pre-existing cracks to close and open, and consequently the seismic velocities decrease and

62 increase in regions of dilatation and contraction of the structure, respectively [e.g. Walsh,

63 1965; Nur, 1971]. For example, seismic velocity changes caused by volcano deformations

64 [Ratdomopurbo and Poupinet, 1995; Nagaoka et al., 2010; Rivet et al., 2014; Donaldson

65 et al., 2017; Takano et al., 2017], thermoelastic strains [Hillers et al., 2015a; Richter et al.,

66 2014; Tsai, 2011] and the Earth tide [Reasenberg and Aki, 1974; Yamamura et al., 2003;

67 Takano et al., 2014; Hillers et al., 2015b], which are not accompanied by strong ground

68 motions, have been observed.

69 Applied strain is one of the above mentioned important mechanisms of velocity

70 changes. We can investigate the mechanical properties of the shallow structure with the

71 strain sensitivity of seismic velocity changes. If seismic velocity changes are observed,

72 we may, for example, monitor a temporal changes of strain in the medium through the

73 strain sensitivity of seismic velocity changes. The Earth tide has been used to estimate

74 the seismic velocity changes in response to the static strain because the tidal strain can be

75 computed accurately. Previous studies have succeeded in detecting the velocity changes

76 correlated well with the tidal strain from temporal changes of travel times of P waves or

77 Rayleigh waves using the artificial controlled sources such as vibrators [De Fazio et al.,

78 1973], air guns [Reasenberg and Aki, 1974], and piezoelectric transducers [Yamamura

et al., 2003]. The strain sensitivity of seismic velocity changes is estimated to range from 1×10^3 to 1×10^5 with these active experiments. In recent years, seismic velocity changes in response to the tidal strain have also been detected by applying a seismic interferometry method to the ambient noise recorded at small seismic arrays [Takano et al., 2014; Hillers et al., 2015b]. Takano et al. [2014] and Hillers et al. [2015b] analyzed CCFs of ambient noises within seismic array stations with apertures of smaller than 500 m. These previous studies pointed out that the sensitivity of velocity changes to the tidal strain is large when analyzing the direct wave part of CCFs. They considered that the tidal strain sensitivity of velocity changes decreases at the coda wave part of CCFs by the contribution of body waves. However, Takano et al. [2014] and Hillers et al. [2015b] did not investigate the wave properties of CCFs at different lapse-times.

We present here the tidal strain sensitivity of seismic velocity changes by the cross-correlation analyses of ambient noise at Izu-Oshima volcano, Japan. In addition, we evaluate wavefield properties of CCFs at different lapse-times by applying an array analysis based on a Richardson-Lucy deconvolution method [Lucy, 1974; Richardson, 1972]. We first analyze the ambient noise between station pairs with the distance ranging from 3 to 8 km at a frequency band of 2 – 4 Hz. Subsequently, we estimate seismic velocity changes in response to the tidal strain at different lapse-times of CCFs. Finally, we apply an array analysis to the CCFs to clarify the wave types in the CCFs with lapse-times.

2 Data

We analyze continuous seismic data recorded by a local seismic network and a small seismic array from 1 April 2014 to 31 March 2015 at Izu-Oshima volcano, an active stratovolcano located at 110 km to the south west of Tokyo, Japan (Figure 1). Earthquakes with magnitudes larger than four have not been observed during this observation period, thus strong ground motion would not affect the observed seismic velocity changes. A local seismic network consists of four short-period (1 Hz) three-component seismic stations with the inter-station distance ranging from about 3 to 8 km, which is maintained by Japan Meteorological Agency (JMA). V.OSFT, V.OSSN and V.OSKT stations are equipped with a borehole-type seismometer at depths of 92 m, 92 m and 61 m, respectively. The seismometer at V.OSMA station is set on the ground surface. The continuous data are recorded with a sampling frequency of 100 Hz and an A/D resolution of 24 bit. At the north eastern part of the volcano, a small seismic array was temporally deployed by National Research

Institute for Earth Science and Disaster Resilience (NIED). The small seismic array consists of seven 1 Hz seismometers and the signals are recorded with a sampling frequency of 200 Hz and an A/D resolution of 27 bit. The seismic array is characterized by an approximately triangular geometry with a diameter of 200 m. Each station in the array is named as the number of station such as OOK1, OOK2,..., OOK7 (see Figure 1). The central station OOK7 has a three-component seismometer and the others have single vertical component seismometer. We analyze only the vertical component of the ambient noise records. We also use a volumetric strain-meter deployed by JMA at a depth of 291 m (see Fig. 1) to estimate the tidal strain at the volcano.

3 Methods

We analyzed the tidal strain first to identify time periods with different strain amplitudes for subsequent seismic ambient noise analysis. We extract the tidal strain by the tidal analysis program Baytap-08 [Tamura *et al.*, 1991] from the raw data of the volumetric strain-meter recorded with a sampling period of 1 hour. The Baytap-08 decomposes the input data into a tidal part, a drift part, a response part and an irregular part. The program then estimate amplitudes and phases of the tidal constituents, a long-term trend, a noise component and a barometric response coefficient by using the Akaike Bayesian information Criterion (ABIC) to select optimum values. The 21 tidal constituents (M2, O1, S2, K1, etc.) are analyzed in this study. We estimate the seismic velocity changes in response to the tidal strain by using CCFs of ambient noise between the seismic network stations and the station located in the middle of the seismic array (OOK7 station). Since coherence among array stations are high and no significant difference is recognized between stations in the array, we use OOK7 as a reference station to calculate the seismic velocity changes.

We calculate seismic velocity changes by measuring phase differences between stacked CCFs during time period with different strain amplitudes following the methods of *Takano et al.* [2014] and *Hillers et al.* [2015b] (Figure 2). This is because we cannot directly compare the tidal strain changes with seismic velocity changes due to the insufficient time resolution of seismic velocity changes. The procedure of data analysis is as follows. Firstly, we apply a narrow bandpass-filter of 2 – 4 Hz to the ambient noises. Secondly, we divide the observational period into five episodes according to the tidal strain amplitudes: (i) more than 4.8×10^{-8} , (ii) more than 1.2×10^{-8} and less than 4.8×10^{-8} , (iii) more than

143 -1.2×10^{-8} and less than 1.2×10^{-8} , (iv) more than -3.2×10^{-8} and less than -1.2×10^{-8} ,
 144 (v) less than -3.2×10^{-8} . We stack CCFs of ambient noise for each episode. The duration
 145 of stacking of CCFs are 1696 hours in episode (i), 1543 hours in episode (ii), 1602 hours
 146 in episode (iii), 1511 hours in episode (iv), and 2408 hours in episode (v). We calculate
 147 CCFs every 10 minutes by applying the one-bit normalization and the spectral whitening
 148 at the frequency band of 2 – 4 Hz [Bensen *et al.*, 2007] to the ambient noise in order to
 149 enhance the signal to noise ratio of CCFs. As can be seen in Fig.S1, the amplitudes of
 150 CCFs in the positive lapse-times are larger than those in the negative lapse-times. The sig-
 151 nals in the positive lapse-time indicates that Rayleigh waves propagate from the OOK7 sta-
 152 tion to the network stations, which suggests that the noise sources are mainly distributed
 153 in the Pacific Ocean (Fig. S3 in supporting information). Thirdly, we compute seismic ve-
 154 locity changes by applying the moving window cross-spectral (MWCS) method [Poupine-
 155 *et al.*, 1984] to the CCFs stacked for episodes with different strain amplitudes, in which
 156 phase differences ($d\varphi$) between CCFs are related to the velocity changes (dv/v) of struc-
 157 ture: $dv/(2\pi fT) = -dv/v$ where T is the lapse time, f is the dominant frequency, and
 158 v is the velocity. We measure seismic velocity changes at the positive and negative lapse
 159 times by 5 s-long 80 % overlapping time windows in lapse-times from 2 s to 30 s. Phase
 160 differences of 1.28 s-long 50 % overlapping time windows with a coherency of more than
 161 0.7 are used for fitting a regression line at each 5 s-long time window. We do not analyze
 162 CCFs with amplitudes close to the background noise level that is estimated from the av-
 163 erage of envelope amplitudes at lapse-time ranging from 290 to 300 s. The envelope am-
 164 plitudes of CCFs in negative lapse time, which are smaller than those in the positive lapse
 165 time, approach the background noise level at lapse-times of 30 s and 50 s at the V.OSSN
 166 station and the others, respectively (Fig. S2). We thus use the CCFs at lapse-time from 2
 167 to 30 s. Finally, we estimate strain sensitivities of seismic velocity changes from the seis-
 168 mic velocity changes versus relative tidal strain differences (Fig. 2c). Strain sensitivities of
 169 velocity changes κ are calculated by:

$$\kappa = \frac{dv/v}{d\epsilon} \quad (1)$$

70 where dv/v indicates the velocity change and $d\epsilon$ the relative strain difference. The relative
 71 tidal strain differences are measured from the averaged strain amplitude at each episode.
 72 We evaluate the tidal strain sensitivity of seismic velocity changes by fitting a linear re-
 73 gression line to the seismic velocity changes against relative tidal strain differences.

174 **4 Result**

175 **4.1 Seismic velocity changes caused by the Earth tide**

176 Strain sensitivities of seismic velocity changes with lapse-times in the 2–4 Hz fre-
 177 quency band are shown in Fig. 3. At lapse-times from about 2 to 7 s, strain sensitivities
 178 are negative for almost all station-pairs (Fig. 4). Since negative strain sensitivity of seis-
 179 mic velocity changes implies that the velocity decreases during dilatation or increases dur-
 180 ing contraction of a medium, the observed seismic velocity changes can be interpreted by
 181 the closing and opening of the cracks in the medium caused by the tidal strain changes,
 182 respectively [e.g. *Walsh*, 1965; *Nur*, 1971; *Yamamura et al.*, 2003]. From the seismic ve-
 183 locity changes at the lapse-times ranging from 2 to 7 s, the strain sensitivity of velocity
 184 changes averaged for four station pairs is estimated to be $(-2.1 \pm 0.2) \times 10^4$. After the
 185 lapse-times of 10 s, the strain sensitivities of seismic velocity changes distribute around
 186 zero value with fluctuations or sometimes in the positive values. The strain sensitivities of
 187 velocity changes show negative values again around the lapse-times ranging from 20 s to
 188 30 s. The reason why strain sensitivities of seismic velocity changes become positive val-
 189 ues is unclear. The positive strain sensitivities of seismic velocity changes recognized at
 190 about 10 s are not matched with opening/closure of cracks in medium, and other unknown
 191 mechanisms are necessary to explain the observation.

192 To obtain averaged characteristics of the strain sensitivity of velocity changes at Izu-
 193 Oshima, we stack the strain sensitivity of velocity changes for the different station-pairs.
 194 We find that the negative strain sensitivity gradually decreases to zero value at the lapse-
 195 times from 2 to 7 s and increase slightly after the lapse-times of 20 s (Fig. 3b). These char-
 196 acteristics are not changed even when a time window of 10 s is used to calculate the seis-
 197 mic velocity changes (Fig. S5).

198 **4.2 Wave properties of CCFs of ambient noise**

199 To understand the mechanism of the lapse-time dependent characteristics of the
 200 strain sensitivity, we estimate the wave properties of CCFs by applying an array analy-
 201 sis to the CCFs. The CCFs are calculated for seismic network stations to all of the ar-
 202 ray stations (OOK1, OOK2,..., OOK7). We take the seismic network stations as virtual
 203 sources. The resolution of array response functions at 2–4 Hz is not so high enough to
 204 estimate the apparent velocity and incident azimuth because the aperture of the array is

close to the wavelength of Rayleigh waves at that frequency. To improve the resolution we deconvolve the array response function from the f-k spectra observed by conventional beamforming methods with the Richardson-Lucy algorithm (see Appendix A for details). Figure 5b shows an example of the deconvolved f-k spectra of CCFs between the V.OSSN station and seismic array stations. At the lapse-times of 2–7 s, the f-k spectrum indicates the apparent velocity of about 1 km/s. Then the apparent velocities become higher than 1 km/s at late lapse-times from 8 s to 30 s. In order to systematically estimate the wave properties of CCFs with lapse-times, we calculate apparent velocities and back-azimuths of CCFs by shifting a time window of 5 s every 1 s at lapse-times ranging from 2 to 30 s (Fig. 6). The time window of 5 s is the same as that we analyzed the lapse-time dependent characteristics of the strain sensitivity in section 4.1. Overall, apparent velocities for all station pairs are about 1 km/s around the direct wave part of CCFs, which is consistent with the group velocity of Rayleigh wave at 1–4 Hz [Takano *et al.*, 2017]. The sensitivity kernel of fundamental Rayleigh waves at the frequency of 3 Hz shows that the depth distribution of strain sensitivity values is shallower than the depth of 0.4 km. For example, at V.OSMA station, the apparent velocities are about 1 km/s at the lapse-times of 2–7 s, and then become higher than 2 km/s at the late lapse-times. From the apparent velocity estimated between each seismic network station and array stations (Fig. 6a), the apparent velocity of V.OSSN are higher than 4 km/s around lapse-times of 10 s. Larger strain sensitivity error bars around lapse time of 10 s might thus be affecting the wave impingement on beneath the array.

These observations are consistent with numerical experiments [Obermann *et al.*, 2013], which show that the sensitivity of coda waves at late lapse-time is contaminated by body waves propagating at deep depths generated by the scattering and wave conversions from surface waves to body waves. From numerical studies by [Obermann *et al.*, 2013], the transition from surface sensitivity to bulk sensitivity in the coda occurs at about six mean free times. In Figure 3b, the transition occurs at about 10 s at the frequency band of 2–4 Hz. This transition time thus provide a transport mean free path of about 1.8 km by assuming a wave speed of 1.1 km/s. Although the transport mean free path has not been determined in the Izu-Oshima volcano, the transport mean free path value is consistent with the values estimated at several active volcanoes [e.g. Yamamoto and Sato, 2010; Prudencio *et al.*, 2017; Wegler and Lühr, 2001]. On the other hand, Maeda *et al.* [2008] synthesized the coda wave envelope propagating through a randomly inhomogeneous medium

in a half-space by considering elastic conversion scattering modes of body-to-body waves, Rayleigh-to-body waves, body-to-Rayleigh waves, and Rayleigh-to-Rayleigh waves based on the Born approximation. *Maeda et al.* [2008] concluded that the scattered body waves are dominant in the coda at high frequencies although Rayleigh-to-Rayleigh scattering mode is dominant in the coda wave envelope at low frequency bands. Our results therefore suggest that the body waves emerge at late lapse-times due to the scattering or reflection of the direct body wave or mode conversion from Rayleigh waves to body waves. *Mikada et al.* [1997] also pointed out a scatterer at a depth of 4–5 km and a larger scatterer at 8–10 km at Izu-Oshima volcano based on a seismic diffraction tomography.

Figure 6b shows incident back azimuths of CCFs as a function of lapse-times. The result does not clearly show the back azimuth of the network station position from the seismic array even at the early lapse-times of 2–7 s. These inconsistencies suggest that the surface structure is very heterogeneous.

Figure 7 illustrates the apparent velocity and strain sensitivity of velocity changes with lapse-times averaged for all the station pairs. Large negative strain sensitivities of velocity changes are observed before the lapse-times of 10 s at which we observe the apparent velocities of about 1 km/s. Strain sensitivities decrease to around zero values at the lapse-times ranging from 10 s to 20 s at which high apparent velocities are observed. After the lapse-time of 20 s, negative strain sensitivities of velocity changes increase again at which the apparent velocities decrease to about 1.5 km/s. Since the shallow part of the structure can be deformed by the Earth tide homogeneously, the depth dependence of seismic velocity changes is controlled by confining pressure [*Mavko et al.*, 2009]. From the granular theory, the strain sensitivity of velocity changes decreases with increasing confining pressure [*Takano et al.*, 2017]. The strain sensitivity of seismic velocity changes therefore decreases at late lapse-times of CCFs due to the contamination of body waves which propagate to deeper parts of the structure, where cracks might be closed by the high confining pressure.

5 Discussion

5.1 Frequency dependent characteristics of the strain sensitivity

Several previous studies have documented the frequency dependence of seismic velocity changes [*Nishimura et al.*, 2005; *Takano et al.*, 2017; *Wu et al.*, 2016; *Rivet et al.*,

269 2011]. *Takano et al.* [2017], for example, reported seismic velocity changes in response to
70 the volcano deformation caused by the pressure source at Izu-Oshima is smaller at 0.375–
271 1 Hz band than those at 1–4 Hz band due to the high confining pressure at the deeper part
272 of structure. We therefore calculate the seismic velocity changes in response to the tidal
273 strain at a frequency band of 1–2 Hz by shifting a time window of 5 s every 1 s from 2 s
274 to 30 s to investigate frequency dependent characteristics of the strain sensitivity. Note
275 that we did not evaluate wave properties of noise correlations at 1–2 Hz band by an array
276 analysis because the wavelength is too long to estimate slowness vectors with a high res-
277 olution. Fig.8 shows the strain sensitivity of seismic velocity changes averaged for four
278 stations at 1–2 Hz and 2–4 Hz. We observe that negative strain sensitivities of seismic ve-
279 locity changes also decrease with increasing lapse-times at 1–2 Hz. After the lapse-times
280 of 25 s, strain sensitivities of seismic velocity changes distribute around zero value. Al-
281 though, the attenuation parameters has not been determined in the shallow structure of
282 Izu-Oshima, we suppose that there is low Q region in the superficial layer at Izu-Oshima.
283 In such case, surface waves with a short period attenuate rapidly while surface waves with
284 a long period are less affected by the low Q region. The frequency dependent charac-
285 teristics of the strain sensitivity therefore may suggest that surface waves are dominant up to
286 the later lapse-times at the lower frequency band. We also analyze the strain sensitivity of
287 seismic velocity changes at 0.5–1 Hz band, but the error of seismic velocity changes is too
288 large to discuss the strain sensitivity of seismic velocity changes.

289 *Takano et al.* [2017] compared the seismic velocity changes with the volcano defor-
290 mation caused by the volcanic pressure source at Izu-Ohsima with the noise correlation
291 method. They estimated the strain sensitivity of velocity changes at 1–2 Hz and 2–4 Hz
292 by fitting a regression line between the seismic velocity changes and areal strain changes
293 which are calculated by displacements of GNSS stations. The strain sensitivity of seis-
294 mic velocity changes, which is caused by the volcano deformation, is averaged for all sta-
295 tion pairs and estimated to be $(-2.0 \pm 1.3) \times 10^3$ at 1–2 Hz and $(-2.1 \pm 1.8) \times 10^3$ at 2–
296 4 Hz when analyzing the CCFs at the lapse-times from -8 to 8 s. On the other hand, the
297 strain sensitivity of velocity changes is estimated to be $(-2.4 \pm 0.1) \times 10^3$ at 1–2 Hz and
298 $(-2.0 \pm 0.1) \times 10^3$ at 2–4 Hz, when analyzing the CCFs at the lapse-times from -20 to
299 20 s. The results indicate that the velocity changes in response to the magma pressure do
300 not vary with lapse-time. This is contrary to the results obtained from the present study
that uses tidal strain. The seismic velocity changes caused by the tidal strain show the

lapse-time dependence, although *Takano et al.* [2017] indicates that the velocity changes in response to the volcano deformation do not vary with the lapse-time. There are three possible causes of differences between the velocity changes in response to the tidal strain and the volcanic pressure source. First, the volcano deformation originates from the pressure source at a depth of about 6 km, and hence areal strains are larger around the pressure source, while tidal strain deforms the volcanic edifice homogeneously. Consequently, the seismic velocity change is sensitive to the volcano deformation even at the late lapse-times because body waves in the late lapse-times may propagate the deeper region around the pressure source. Second, *Takano et al.* [2017] compute CCFs between the seismic network stations, while we compute CCFs between the seismic network stations and OOK7 station at the seismic array. The differences of strain sensitivity suggest that the strain sensitivity varies in different regions even within the volcano. However, since we analyzed only four station pairs, it is difficult to discuss the spatial distribution of the estimated strain sensitivity with the geological structure of Izu-Oshima volcano. We need to deploy more seismic stations Izu-Oshima to investigate a characteristic of spatial distribution of strain sensitivities. Third, the duration of stacking CCFs is different. We stack CCFs for about 70 days at each period, on the other hand, *Takano et al.* [2017] stack CCFs for 20 days. The seismic velocity changes caused by the volcano deformation when analyzing the direct wave part may be affected by noise distribution variations due to the insufficiency of the stacking.

5.2 Seismic velocity changes caused by the tidal strain within the small seismic array

In order to verify the magnitude of the strain sensitivity, we estimate seismic velocity changes between the seismic array stations as done in *Takano et al.* [2014] and *Hillers et al.* [2015b]. We measure velocity changes by shifting a time window of 5 s every 1 s at the positive and negative lapse-times ranging from 0 s to 30 s. We investigate here only the seismic velocity changes at the frequency bands of 1–2 Hz and 2–4 Hz because wavelengths at frequencies below 1 Hz are too long for the inter-station distance of the array stations. Strain sensitivity stacked for 21 station-pairs shows that negative strain sensitivities of seismic velocity changes decreases with increasing lapse-times at 1–2 Hz and 2–4 Hz: strain sensitivities decrease after 15 s at 1–2 Hz, and 10 s at 2–4 Hz (Fig. 9). These results suggest that seismic velocity changes are sensitive to the tidal strain not only be-

334 tween seismic network stations and the seismic array but also at the localized area around
335 the seismic array. The strain sensitivity of seismic velocity changes is comparable to the
336 averaged strain sensitivity obtained at the lapse-times of 2–7 s between the network sta-
337 tions and the seismic array at 2–4 Hz. On the other hand, at 1–2 Hz, the strain sensitivity
338 determined by the array only is almost consistent with that estimated by the station pair of
339 V.OSSN and OOK7 and less than about 4 times of the other pairs.

340 We compare the strain sensitivity of velocity changes with the previous studies which
341 applied noise correlation technique to the ambient noise data recorded at the small seismic
342 arrays at the foot of the Iwate volcano, Japan [Takano *et al.*, 2014], and the San Jacinto
343 Mountains, Southern California [Hillers *et al.*, 2015b]. The previous studies analyzed the
344 direct wave part of CCFs to estimate the seismic velocity changes. The strain sensitivity
345 of velocity changes were estimated to be 6.9×10^4 at a frequency band of 1–2 Hz and
346 -5×10^3 at a frequency band of 2–8 Hz, respectively, from the seismic velocity changes
347 in response to the tidal strain. On the other hand, the strain sensitivity of seismic veloc-
348 ity changes at Izu-Oshima when analyzing the lapse-times ranging from -6 to 6 s, which
349 corresponds to the direct wave part of CCFs, are estimated to be $(-0.8 \pm 0.3) \times 10^4$ at
350 1–2 Hz and $(-2.3 \pm 0.3) \times 10^4$ at 2–4 Hz. The magnitude of strain sensitivities obtained
351 in this study are within a range of previous results. Previous observations [Takano *et al.*,
352 2014; Reasenberg and Aki, 1974; Yamamura *et al.*, 2003] reported that velocity decreases
353 during dilatation or increases during contraction of a medium by the Earth tide, which is
354 consistent with the polarity of strain sensitivity at early lapse-times in this study. How-
355 ever, Hillers *et al.* [2015b] showed opposite polarity of strain sensitivity to previous studies
356 [Takano *et al.*, 2014; Reasenberg and Aki, 1974; Yamamura *et al.*, 2003] and this study.

357 5.3 Effect of diurnal variations on seismic velocity changes

358 Previous studies indicate that seismic velocity changes are also sensitive to the di-
359urnal variations such as atmospheric temperature changes [Hillers *et al.*, 2015a; Richter
360 *et al.*, 2014; Tsai, 2011] and noise source distribution changes [Froment *et al.*, 2010; Weaver
361 *et al.*, 2009]. Hillers *et al.* [2015a], for example, shows that the thermoelastic strain is the
362 possible mechanism for the seasonal velocity changes observed in the San Jacinto fault
363 area by the correlation and phase differences between velocity changes and atmospheric
364 temperature changes. Thermoelastic strains at given depths induced by surface tempera-
365 ture changes for a 2-D elastic half-space were derived by Berger [1975]. The areal strain

amplitude at the depth of 1 km by the diurnal temperature changes of 4°C at Izu-Oshima with a spatial wavelength of 10 km is estimated to be about 3×10^{-8} . We estimate the areal strain by assuming that the coefficient of thermal expansion and the thermal diffusivity is $10^{-5}^{\circ}\text{C}^{-1}$ and $10^{-6}\text{m}^2/\text{s}$, respectively, which are used in Berger [1975]. Since the tidal strain amplitude is 1.2×10^{-7} at Izu-Oshima, thermoelastic strain may affect about from 20 % to 30 % of our estimation. In addition, variations of noise source distribution also cause apparent velocity changes of several percentages especially at the direct wave part of CCFs [Froment *et al.*, 2010]. Apparent travel time shift occurs by a relationship between the direction of seismic noise wavefield and the station pair. We therefore estimate the velocity changes in response to the tidal strain by avoiding the effect of diurnal changes except for the Earth tide in this section.

Most of the seismic data in the dilatational episode (more than 1.2×10^{-8}) are distributed around midnight and noon in the local time, on the other hand the data in the contraction period (less than -1.2×10^{-8}) are distributed around 6 p.m. and 6 a.m. (Fig. 10a). In order to avoid the effect of diurnal variations on the seismic velocity changes, we measure the seismic velocity changes by the cross-correlations of ambient noises in a fixed time window of 12 hours long (0–6 h and 18–24 h). We analyze only the lapse-time from 2 to 7 s of CCFs. The results (Figure 13b) show that the seismic velocity changes are related to tidal strain when only these selected data are analyzed. Furthermore, we estimate the strain sensitivity of seismic velocity changes by shifting a time window of 12 hours every 2 hours (Fig. 10c). Almost all strain sensitivities of velocity changes distributed around -1.0×10^4 . Average strain sensitivity is estimated to be $(-0.8 \pm 0.5) \times 10^4$, which is consistent with the strain sensitivity calculated by the ambient noise stacked in the whole observational period. We therefore conclude that diurnal variations, apart from Earth tides, do not have a large influence on the observed strain sensitivity of seismic velocity changes at Izu-Oshima.

6 Conclusion

We have examined the seismic velocity changes in response to the tidal strain with a noise correlation method at Izu-Oshima volcano, Japan. To estimate velocity changes in response to the tidal strain, we measure phase differences between CCFs of ambient noises stacked for time periods with different tidal strain amplitudes. From the seismic velocity changes against relative tidal strain differences, we compute strain sensitivity of the

398 seismic velocity changes at different lapse-times of CCFs. We find negative strain sensitivities
 399 when analyzing the CCFs at the lapse-times ranging from 2 to 7 s, which suggest that
 400 the observed seismic velocity changes can be explained by the closing and opening of the
 401 cracks in the medium caused by the tidal strain. The magnitude of the strain sensitivity
 402 decreases when analyzing CCFs at late lapse-times from 7 to 35 s.

403 To understand these characteristics, we investigated the wave properties of CCFs by
 404 applying the array analysis. High resolution analyses of f-k spectra indicate the apparent
 405 velocities of about 1 km/s at the lapse-times of 10 s and those of higher than 1 km/s at
 406 later than lapse-times of 10 s. Since the group velocity of Rayleigh wave at 2 – 4 Hz is
 407 about 1 km/s at Izu-Oshima, apparent velocities of higher than 1 km/s suggest that body
 408 waves emerge at the late lapse-times by scattering or reflecting from direct body waves
 409 or surface waves. Therefore, we conclude that the strain sensitivity of seismic velocity
 410 changes decreases at late lapse-times due to the contamination of body waves which prop-
 411 agate deeper part of the structure where cracks may be closed due to the high confining
 412 pressure. These results show that identifying different wave types contained in CCFs is
 413 important to accurately interpret seismic velocity changes.

414 **Figure 1.** Locations of seismic stations (blue inverted triangles), a seismic array (brown circles), and a
 415 strain-meter (purple circle).

416
 417 **Figure 2.** Procedures of the analysis. (a) Tidal strain are extracted from the raw data of the volumetric
 418 strain-meter by the Baytap-08. (b) Cross-correlations are stacked in each episode between V.OSFT station
 419 and OOK7 station. (c) Schematic illustration of seismic velocity changes are estimated from the CCFs in each
 420 episode pair. The rightmost open circle, for example, shows the velocity change estimated from the CCF in
 episode (i) with respect to episode (v). Dashed line show a linear fitting to the seismic velocity changes.

421
 422 **Figure 3.** (a) Strain sensitivity of seismic velocity changes at different lapse time with the time window
 423 length of 5 s at the frequency band of 2–4 Hz. Error bars show one standard deviation. (b) Lapse time depen-
 dence of strain sensitivity that are averaged for four station-pairs at the frequency band of 2–4 Hz.

Figure 4. (a) Seismic velocity changes versus relative tidal strain difference averaged for four station-pairs at the frequency band of 2–4 Hz when analyzing the lapse-times from 2 to 7 s. (b) Spatial distribution of the strain sensitivity of velocity changes.

Figure 5. (a)CCFs of ambient noise between V.OSSN and OOK7. (b) Deconvolved f-k spectra of the CCF at the lapse-times of 2–7 s, 8–13 s, 16–21 s, and 25–30 s.

Figure 6. (a) Apparent velocity calculated by the array analysis at the station pair between each network station and seismic array. Black horizontal lines indicate the velocity of 1.1 km/s, which corresponds to the fundamental mode of Rayleigh-wave velocity at Izu-Oshima. Open circles indicate starting points of the time window of 5 s. Dotted lines indicate the arrival time of the direct wave, which is calculated by the inter-station distance and Rayleigh-wave velocity of 1.1 km/s. At V.OSSN stations, the data at the lapse-times from 8 to 10 s are not shown because the apparent velocity is higher than 4 km/s. (b) Backazimuths at the station pairs between each network station and the seismic array station. 0 and 90 degree represents North and East, respectively. Open circles indicate starting points of the time window of 5 s. Dotted lines indicate the arrival time of the direct surface wave, which is calculated by the inter-station distance and Rayleigh-wave velocity of 1.1 km/s.

Figure 7. Averaged apparent velocities for all station with error bars.

Figure 8. Averaged strain sensitivities of seismic velocity changes at different lapse-times at the frequency band of 1–2 Hz (a) and 2–4 Hz (b).

Figure 9. Strain sensitivity of seismic velocity changes within the seismic array at different lapse time at the frequency band of 1–2 Hz (a) and 2–4 Hz (b).

Figure 10. (a) Total durations of dilatational episodes (red bars) and contractional episodes (blue bars) for each hour of the day during our observational period. Yellow bars show the duration of episodes with strain ranges from -1.2×10^{-8} to 1.2×10^{-8} (b) Seismic velocity changes versus relative tidal strain differences averaged for four station-pairs by stacking the CCFs in a night time window (Gray shaded areas in Fig. 10a). (c) Strain sensitivity of velocity changes by shifting a time window of 12 hours every 2 hours.

Acknowledgments

We thank the Japan Meteorological Agency for providing us with continuous seismic data which were from the Data management Center of National Research Institute for Earth Science and Disaster Resilience (<http://www.hinet.bosai.go.jp>) and volumetric strain data

(<http://www.data.jma.go.jp>). All figures were made using the Generic Mapping Tool [Wessel and Smith, 1998]. Careful and constructive comments from reviewer Anne Obermann and an anonymous reviewer significantly improved this manuscript. We thank the Editor Martha Savage and the Associate Editor Gregory Waite for editorial efforts and comments. Tomoya Takano is grateful for support from the Japan Society for the Promotion of Science (JSPS) and a partial support from the Ministry of Education, Culture, Sports, Science and Technology (MEXT) of Japan, under its Earthquake and Volcano Hazards Observation and Research Program.

References

- Bensen, G. D., M. H. Ritzwoller, M. P. Barmin, A. L. Levshin, F. Lin, M. P. Moschetti, N. M. Shapiro, and Y. Yang (2007), Processing seismic ambient noise data to obtain reliable broad-band surface wave dispersion measurements, *Geophysical Journal International*, 169(3), 1239–1260, doi:10.1111/j.1365-246X.2007.03374.x.
- Berger, J. (1975), A note on thermoelastic strains and tilts, *Journal of Geophysical Research*, 80(2), 274–277, doi:10.1029/JB080i002p00274.
- Brenguier, F., M. Campillo, C. Hadzioannou, N. M. Shapiro, R. M. Nadeau, and E. Larose (2008), Postseismic relaxation along the san andreas fault at parkfield from continuous seismological observations, *Science*, 321(5895), 1478–1481, doi:10.1126/science.1160943.
- De Fazio, T. L., K. Aki, and J. Alba (1973), Solid earth tide and observed change in the in situ seismic velocity, *Journal of Geophysical Research*, 78(8), 1319–1322, doi:10.1029/JB078i008p01319.
- Donaldson, C., C. Caudron, R. G. Green, W. A. Thelen, and R. S. White (2017), Relative seismic velocity variations correlate with deformation at kilauea volcano, *Science Advances*, 3(6), doi:10.1126/sciadv.1700219.
- Froment, B., M. Campillo, P. Roux, P. Gouédard, A. Verdel, and R. L. Weaver (2010), Estimation of the effect of nonisotropically distributed energy on the apparent arrival time in correlations, *GEOPHYSICS*, 75(5), SA85–SA93, doi:10.1190/1.3483102.
- Hillers, G., Y. Ben-Zion, M. Campillo, and D. Zigone (2015a), Seasonal variations of seismic velocities in the san jacinto fault area observed with ambient seismic noise, *Geophysical Journal International*, 202(2), 920–932, doi:10.1093/gji/ggv151.

- Hillers, G., L. Retailleau, M. Campillo, A. Inbal, J.-P. Ampuero, and T. Nishimura (2015b), In situ observations of velocity changes in response to tidal deformation from analysis of the high-frequency ambient wavefield, *Journal of Geophysical Research: Solid Earth*, 120(1), 210–225, doi:10.1002/2014JB011318, 2014JB011318.
- Lucy, L. B. (1974), An iterative technique for the rectification of observed distributions, *The Astronomical Journal*, 79(6), 745–754.
- Maeda, T., H. Sato, and T. Nishimura (2008), Synthesis of coda wave envelopes in randomly inhomogeneous elastic media in a half-space: single scattering model including rayleigh waves, *Geophysical Journal International*, 172(1), 130–154, doi:10.1111/j.1365-246X.2007.03603.x.
- Mavko, G., T. Mukerji, and J. Dvorkin (2009), *The Rock Physics Handbook: Tools for Seismic Analysis of Porous Media*, 2 ed., Cambridge University Press, doi: 10.1017/CBO9780511626753.
- Meier, U., N. M. Shapiro, and F. Brenguier (2010), Detecting seasonal variations in seismic velocities within los angeles basin from correlations of ambient seismic noise, *Geophysical Journal International*, 181(2), 985–996.
- Mikada, H., H. Watanabe, and S. Sakashita (1997), Evidence for subsurface magma bodies beneath izu-oshima volcano inferred from a seismic scattering analysis and possible interpretation of the magma plumbing system of the 1986 eruptive activity, *Physics of the Earth and Planetary Interiors*, 104(1), 257 – 269, doi:[https://doi.org/10.1016/S0031-9201\(97\)00060-5](https://doi.org/10.1016/S0031-9201(97)00060-5), stochastic Seismology Stochastic Seismic Wave Fields and Realistic Media.
- Nagaoka, Y., K. Nishida, Y. Aoki, and M. Takeo (2010), Temporal change of phase velocity beneath mt. asama, japan, inferred from coda wave interferometry, *Geophysical Research Letters*, 37(22), n/a–n/a, doi:10.1029/2010GL045289, l22311.
- Nakata, N., and R. Snieder (2012), Estimating near-surface shear wave velocities in japan by applying seismic interferometry to kik-net data, *Journal of Geophysical Research: Solid Earth*, 117(B1), n/a–n/a, doi:10.1029/2011JB008595, b01308.
- Nishimura, T., S. Tanaka, T. Yamawaki, H. Yamamoto, T. Sano, M. Sato, H. Nakahara, N. Uchida, S. Hori, and H. Sato (2005), Temporal changes in seismic velocity of the crust around iwate volcano, japan, as inferred from analyses of repeated active seismic experiment data from 1998 to 2003, *Earth, Planets and Space*, 57(6), 491–505, doi:10.1186/BF03352583.

- Nur, A. (1971), Effects of stress on velocity anisotropy in rocks with cracks, *Journal of Geophysical Research*, 76(8), 2022–2034.
- Obermann, A., T. Planès, E. Larose, C. Sens-Schönfelder, and M. Campillo (2013), Depth sensitivity of seismic coda waves to velocity perturbations in an elastic heterogeneous medium, *Geophysical Journal International*, 194(1), 372–382, doi:10.1093/gji/ggt043.
- Peng, Z., and Y. Ben-Zion (2006), Temporal changes of shallow seismic velocity around the karadere-düzce branch of the north anatolian fault and strong ground motion, *pure and applied geophysics*, 163(2), 567–600, doi:10.1007/s00024-005-0034-6.
- Poupinet, G., W. L. Ellsworth, and J. Frechet (1984), Monitoring velocity variations in the crust using earthquake doublets: An application to the calaveras fault, california, *Journal of Geophysical Research: Solid Earth*, 89(B7), 5719–5731, doi: 10.1029/JB089iB07p05719.
- Prudencio, J., Y. Aoki, M. Takeo, J. M. Ibáñez, E. Del Pezzo, and W. Song (2017), Separation of scattering and intrinsic attenuation at asama volcano (japan): Evidence of high volcanic structural contrasts, *Journal of Volcanology and Geothermal Research*, 333, 96–103.
- Ratdomopurbo, A., and G. Poupinet (1995), Monitoring a temporal change of seismic velocity in a volcano: Application to the 1992 eruption of mt. merapi (indonesia), *Geophysical Research Letters*, 22(7), 775–778, doi:10.1029/95GL00302.
- Reasenberg, P., and K. Aki (1974), A precise, continuous measurement of seismic velocity for monitoring in situ stress, *Journal of Geophysical Research*, 79(2), 399–406, doi: 10.1029/JB079i002p00399.
- Richardson, W. H. (1972), Bayesian-based iterative method of image restoration*, *J. Opt. Soc. Am.*, 62(1), 55–59, doi:10.1364/JOSA.62.000055.
- Richter, T., C. Sens-Schönfelder, R. Kind, and G. Asch (2014), Comprehensive observation and modeling of earthquake and temperature-related seismic velocity changes in northern chile with passive image interferometry, *Journal of Geophysical Research: Solid Earth*, 119(6), 4747–4765.
- Rivet, D., M. Campillo, N. M. Shapiro, V. Cruz-Atienza, M. Radiguet, N. Cotte, and V. Kostoglodov (2011), Seismic evidence of nonlinear crustal deformation during a large slow slip event in mexico, *Geophysical Research Letters*, 38(8), n/a–n/a, doi: 10.1029/2011GL047151, l08308.

- 549 Rivet, D., F. Brenguier, D. Clarke, N. M. Shapiro, and A. Peltier (2014), Long-term dy-
550 namics of piton de la fournaise volcano from 13 years of seismic velocity change mea-
551 surements and gps observations, *Journal of Geophysical Research: Solid Earth*, 119(10),
552 7654–7666.
- 553 Rivet, D., F. Brenguier, and F. Cappa (2015), Improved detection of preeruptive seis-
554 mic velocity drops at the piton de la fournaise volcano, *Geophysical Research Letters*,
555 42(15), 6332–6339.
- 556 Rost, S., and C. Thomas (2002), Array seismology: Methods and applications, *Reviews of*
557 *Geophysics*, 40(3), 2–1–2–27, doi:10.1029/2000RG000100, 1008.
- 558 Rubinstein, J. L., and G. C. Beroza (2004), Evidence for widespread nonlinear strong
559 ground motion in the mw 6.9 loma prieta earthquake, *Bulletin of the Seismological Soci-*
560 *ety of America*, 94(5), 1595, doi:10.1785/012004009.
- 561 Rubinstein, J. L., and G. C. Beroza (2005), Depth constraints on nonlinear strong ground
562 motion from the 2004 parkfield earthquake, *Geophysical Research Letters*, 32(14), n/a–
563 n/a, doi:10.1029/2005GL023189, 114313.
- 564 Sawazaki, K., H. Sato, H. Nakahara, and T. Nishimura (2006), Temporal change in site
565 response caused by earthquake strong motion as revealed from coda spectral ratio mea-
566 surement, *Geophysical research letters*, 33(21).
- 567 Sawazaki, K., H. Sato, H. Nakahara, and T. Nishimura (2009), Time-lapse changes of
568 seismic velocity in the shallow ground caused by strong ground motion shock of the
569 2000 western-tottori earthquake, japan, as revealed from coda deconvolution analysis–
70 changes of seismic velocity caused by strong ground motion shock of 2000 western-
tottori earthquake, *Bulletin of the Seismological Society of America*, 99(1), 352, doi:
572 10.1785/0120080058.
- 573 Sens-Schönfelder, C., and U. Wegler (2006), Passive image interferometry and seasonal
574 variations of seismic velocities at merapi volcano, indonesia, *Geophysical Research Let-*
575 *ters*, 33(21), n/a–n/a, doi:10.1029/2006GL027797, 121302.
- 576 Snieder, R. (2004), Extracting the green's function from the correlation of coda
577 waves: A derivation based on stationary phase, *Phys. Rev. E*, 69, 046,610, doi:
78 10.1103/PhysRevE.69.046610.
- 579 Snieder, R., A. Grêt, H. Douma, and J. Scales (2002), Coda wave interferometry for es-
580 timating nonlinear behavior in seismic velocity, *Science*, 295(5563), 2253–2255, doi:
581 10.1126/science.1070015.

- 582 Takagi, R., T. Okada, H. Nakahara, N. Umino, and A. Hasegawa (2012), Coseismic
583 velocity change in and around the focal region of the 2008 iwa-te-miyagi nairiku
584 earthquake, *Journal of Geophysical Research: Solid Earth*, 117(B6), n/a–n/a, doi:
585 10.1029/2012JB009252, b06315.
- 586 Takano, T., T. Nishimura, H. Nakahara, Y. Ohta, and S. Tanaka (2014), Seismic velocity
587 changes caused by the earth tide: Ambient noise correlation analyses of small-array
588 data, *Geophysical Research Letters*, 41(17), 6131–6136, doi:10.1002/2014GL060690,
589 2014GL060690.
- 590 Takano, T., T. Nishimura, and H. Nakahara (2017), Seismic velocity changes concentrated
591 at the shallow structure as inferred from correlation analyses of ambient noise during
592 volcano deformation at izu-oshima, japan, *Journal of Geophysical Research: Solid Earth*,
593 122(8), 6721–6736, doi:10.1002/2017JB014340, 2017JB014340.
- 594 Tamura, Y., T. Sato, M. Ooe, and M. Ishiguro (1991), A procedure for tidal analysis with
595 a bayesian information criterion, *Geophysical Journal International*, 104(3), 507–516,
596 doi:10.1111/j.1365-246X.1991.tb05697.x.
- 597 Tsai, V. C. (2011), A model for seasonal changes in gps positions and seismic wave
598 speeds due to thermoelastic and hydrologic variations, *Journal of Geophysical Research:*
599 *Solid Earth*, 116(B4), n/a–n/a, doi:10.1029/2010JB008156, b04404.
- 600 Walsh, J. B. (1965), The effect of cracks on the compressibility of rock, *Journal of Geo-*
601 *physical Research*, 70(2), 381–389, doi:10.1029/JZ070i002p00381.
- 602 Wang, Q.-Y., F. Brenguier, M. Campillo, A. Lecointre, T. Takeda, and Y. Aoki (2017),
603 Seasonal crustal seismic velocity changes throughout japan, *Journal of Geophysical Re-*
604 *search: Solid Earth*, 122(10), 7987–8002, doi:10.1002/2017JB014307, 2017JB014307.
- 605 Weaver, R., B. Froment, and M. Campillo (2009), On the correlation of non-isotropically
606 distributed ballistic scalar diffuse waves, *The Journal of the Acoustical Society of Amer-*
607 *ica*, 126(4), 1817–1826, doi:10.1121/1.3203359.
- 608 Weaver, R. L., and O. I. Lobkis (2001), Ultrasonics without a source: Thermal
609 fluctuation correlations at mhz frequencies, *Phys. Rev. Lett.*, 87, 134,301, doi:
610 10.1103/PhysRevLett.87.134301.
- 611 Wegler, U., and B. G. Lühr (2001), Scattering behaviour at merapi volcano (java) revealed
612 from an active seismic experiment, *Geophysical Journal International*, 145(3), 579–592.
- 613 Wegler, U., H. Nakahara, C. Sens-Schönfelder, M. Korn, and K. Shiomi (2009), Sud-
614 den drop of seismic velocity after the 2004 mw 6.6 mid-niigata earthquake, japan, ob-

- served with passive image interferometry, *Journal of Geophysical Research: Solid Earth*, 114(B6), n/a–n/a, doi:10.1029/2008JB005869, b06305.
- Wessel, P., and W. H. F. Smith (1998), New, improved version of generic mapping tools released, *Eos, Transactions American Geophysical Union*, 79(47), 579–579, doi: 10.1029/98EO00426.
- Wu, C., A. Delorey, F. Brenguier, C. Hadzioannou, E. G. Daub, and P. Johnson (2016), Constraining depth range of s wave velocity decrease after large earthquakes near park-field, California, *Geophysical Research Letters*, 43(12), 6129–6136.
- Yamamoto, M., and H. Sato (2010), Multiple scattering and mode conversion revealed by an active seismic experiment at Asama volcano, Japan, *Journal of Geophysical Research: Solid Earth*, 115(B7), doi:10.1029/2009JB007109.
- Yamamura, K., O. Sano, H. Utada, Y. Takei, S. Nakao, and Y. Fukao (2003), Long-term observation of in situ seismic velocity and attenuation, *Journal of Geophysical Research: Solid Earth*, 108(B6), n/a–n/a, doi:10.1029/2002JB002005, 2317.

A: Richardson-Lucy deconvolution

Fig.A.1 shows the array response function of the seismic array at Izu-Oshima. The main lobe of the array response function ranges from -0.5 to 0.5 s/km (Fig.A.1). This is because the aperture of the seismic array is comparable with the half of maximum wavelength of Rayleigh wave at the frequency band of 2 – 4 Hz. In order to enhance the resolution of the beamformer outputs, we apply the Richardson-Lucy deconvolution method [Lucy, 1974; Richardson, 1972] to the images obtained by the conventional beamforming analysis [Rost and Thomas, 2002].

The deblurring image is constructed by the iterative equation based on a Bayesian framework

$$O_{i+1}(\mathbf{p}) = O_i(\mathbf{p}) \left[P(\mathbf{p})^T * \frac{I(\mathbf{p})}{P(\mathbf{p}) * O_i(\mathbf{p})} \right] \quad (\text{A.1})$$

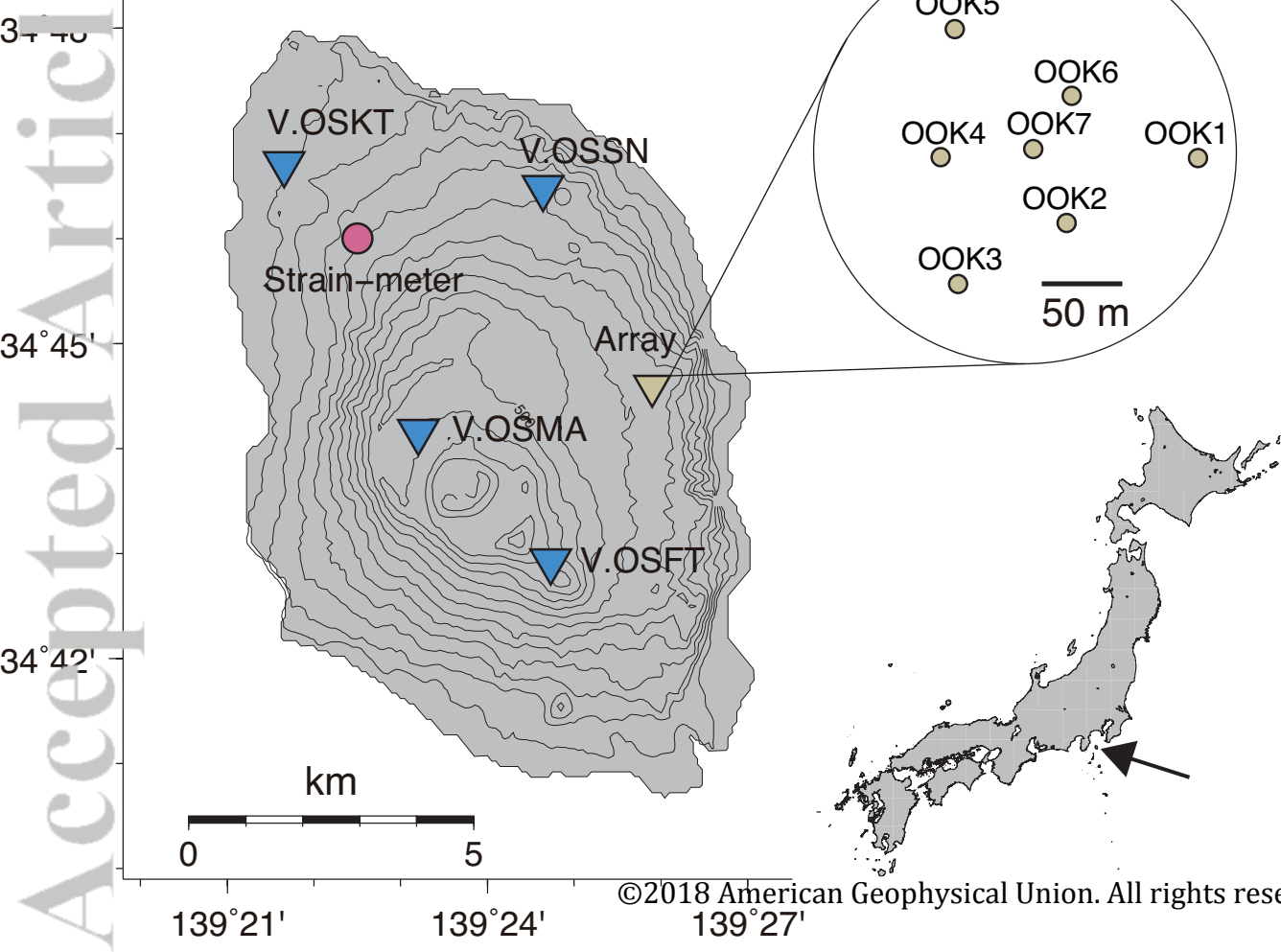
where T stands for transposition, \mathbf{p} denotes slowness vector, i denotes the iteration number, $P(\mathbf{p})$ is the array response function, $O(\mathbf{p})$ is the original noise-free image, and $I(\mathbf{p})$ is an observed image. In our analysis, we set the $O_0(\mathbf{p})$ to be 0.5. This equation iteratively deconvolves the array response function under a maximum likelihood constraint assuming the blurred image follows the Poisson distribution. We extend each image by zero padding to avoid the boundary effects due to the Gibbs oscillations. We perform a

synthetic test to characterize the Richardson-Lucy deconvolution algorithm. The synthetic test is made for the geometry of the seismic array at Izu-Oshima. We consider one plane wave with the velocity of 1 km/s and frequency of 3 Hz. We set the incident azimuth of the wave to 135°. We use 150 iterations for the deconvolution. Fig.A.2 illustrates that the f-k spectrum of the synthetic plane wave by the conventional beamforming and the Richardson-Lucy deconvolution method. The resolution of the f-k spectra is enhanced by the Richardson-Lucy deconvolution method.

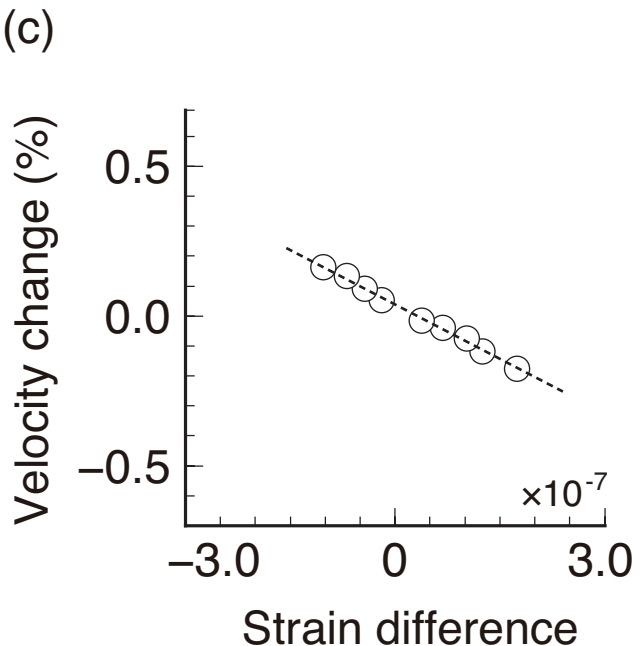
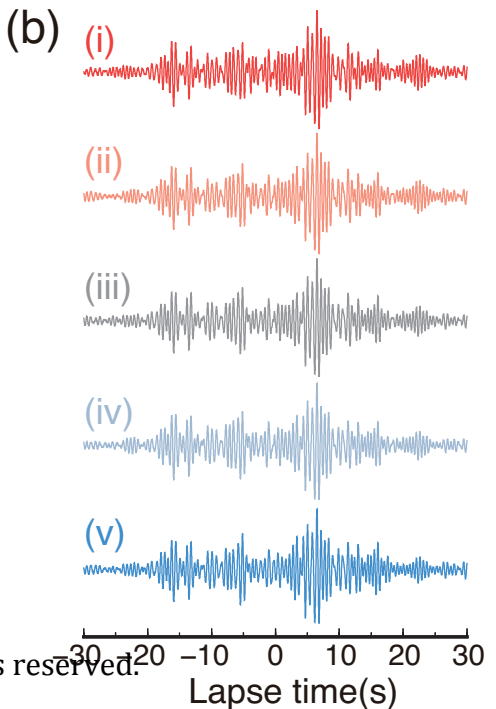
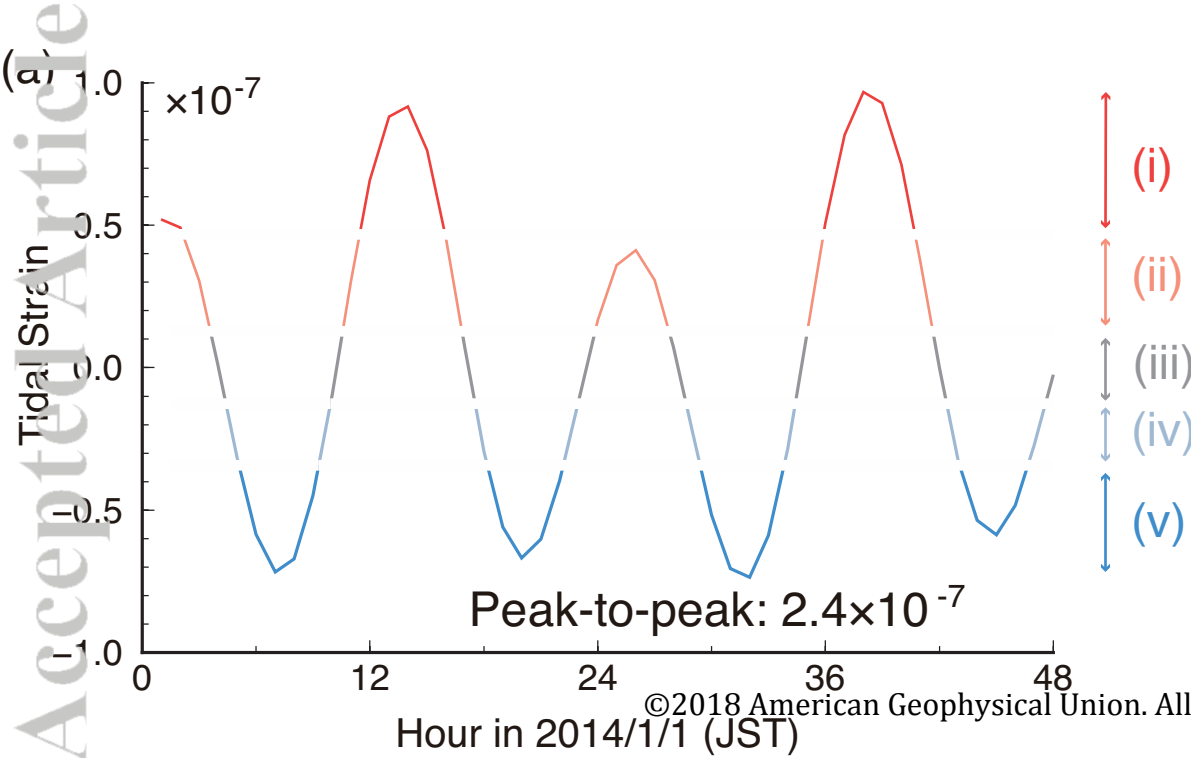
Figure A.1. Array response function of the seismic array computed at the frequency band of 2 – 4 Hz. Contour lines are plotted every 2 dB. Blue broken lines show 2 km/s and 1 km/s, respectively.

Figure A.2. Comparison between (a) conventional beamforming and (b) Richardson-Lucy deconvolution algorithm.

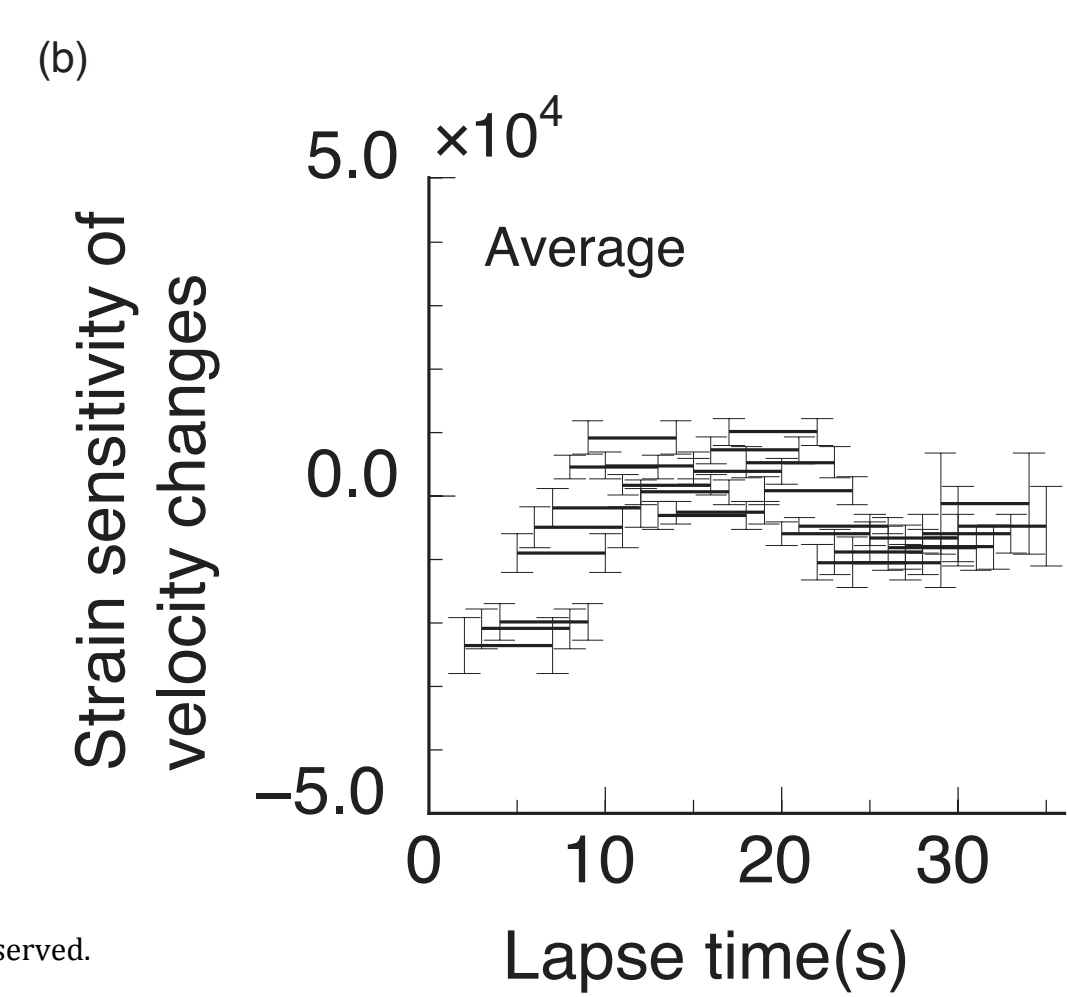
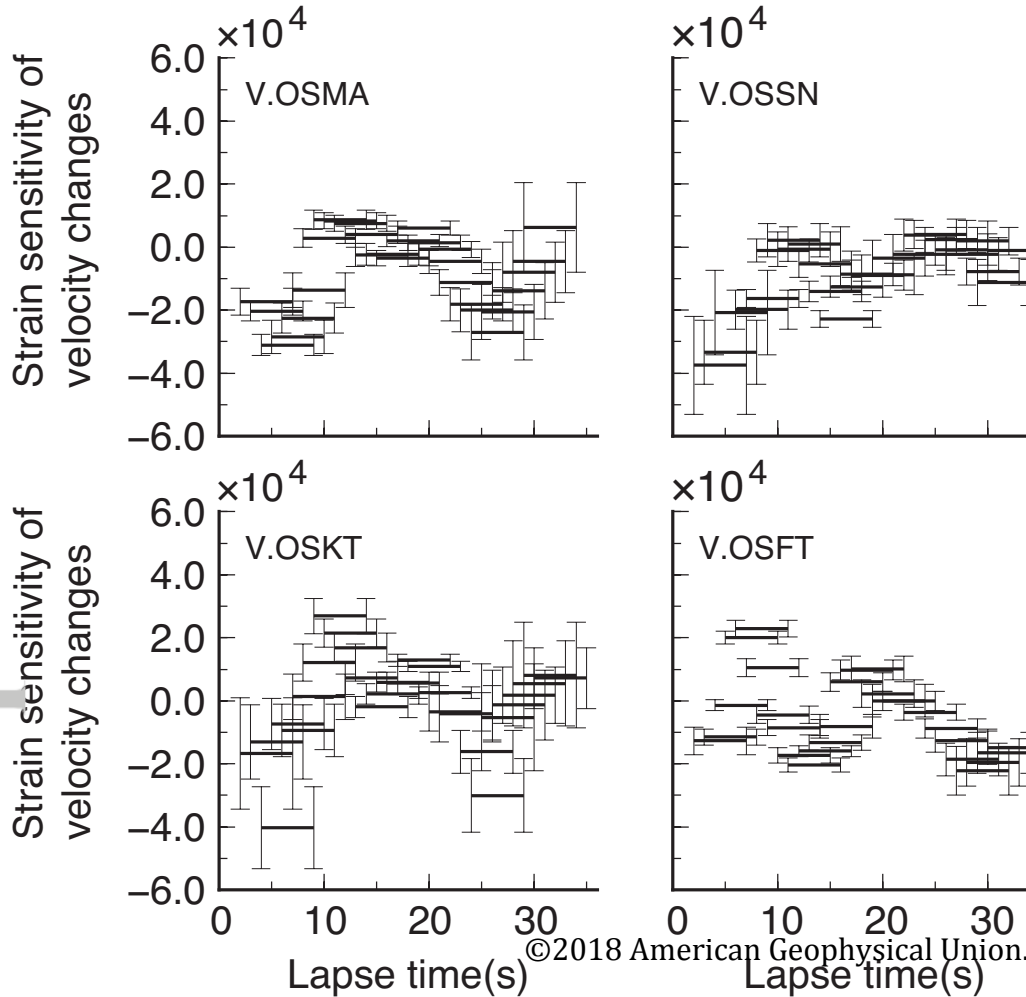
Accepted Article



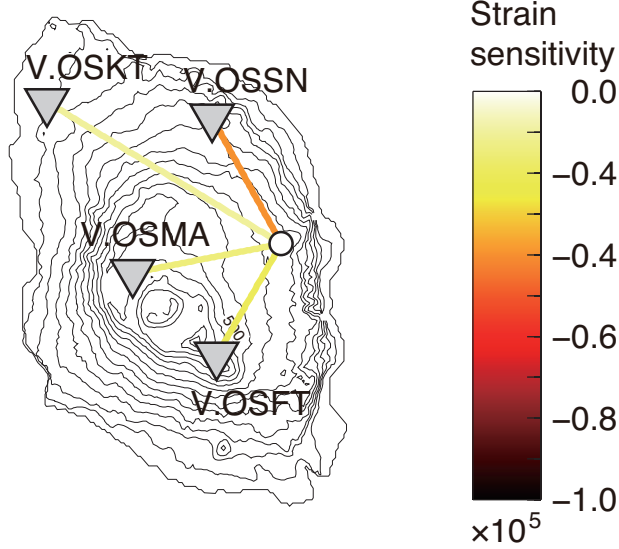
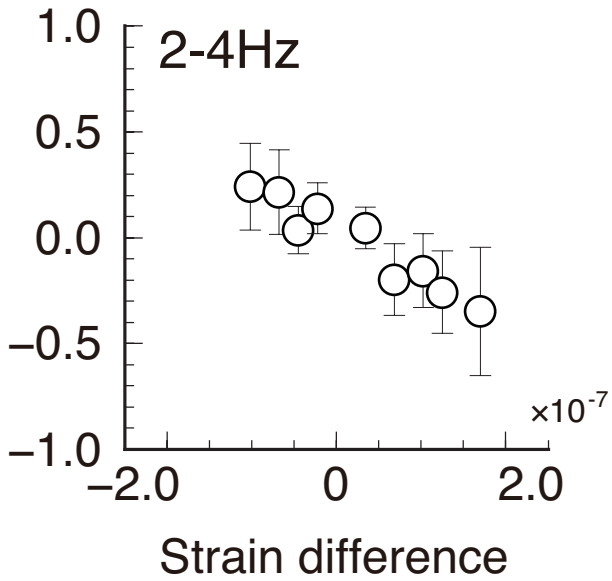
Accepted Article



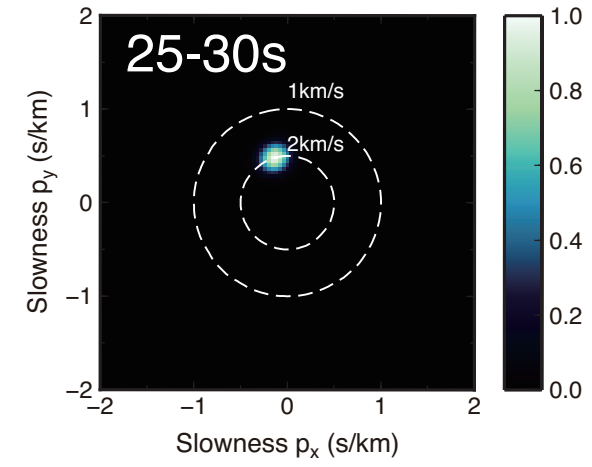
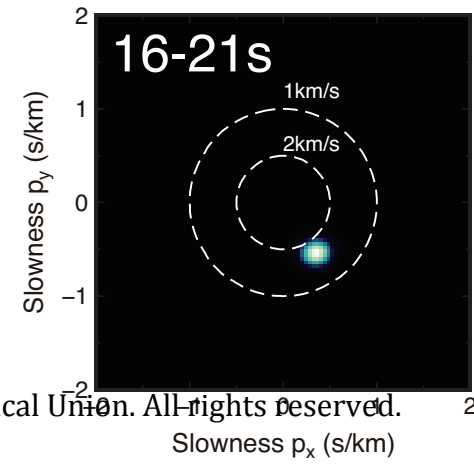
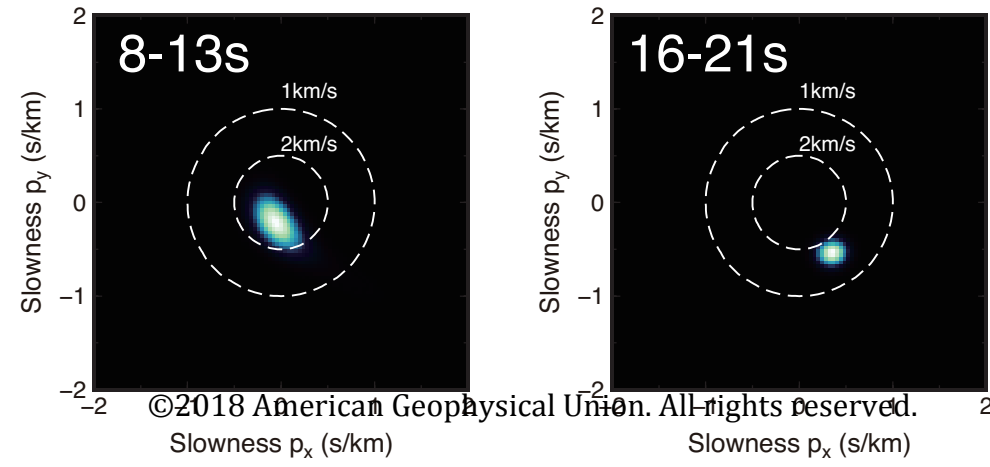
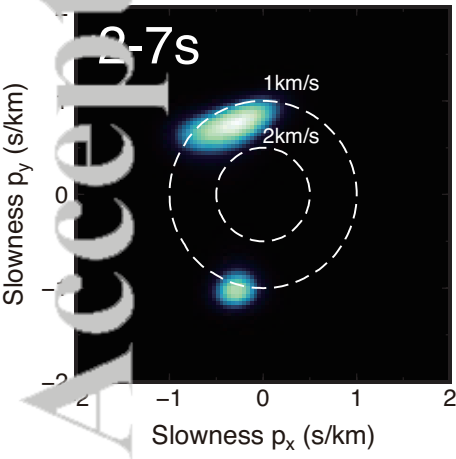
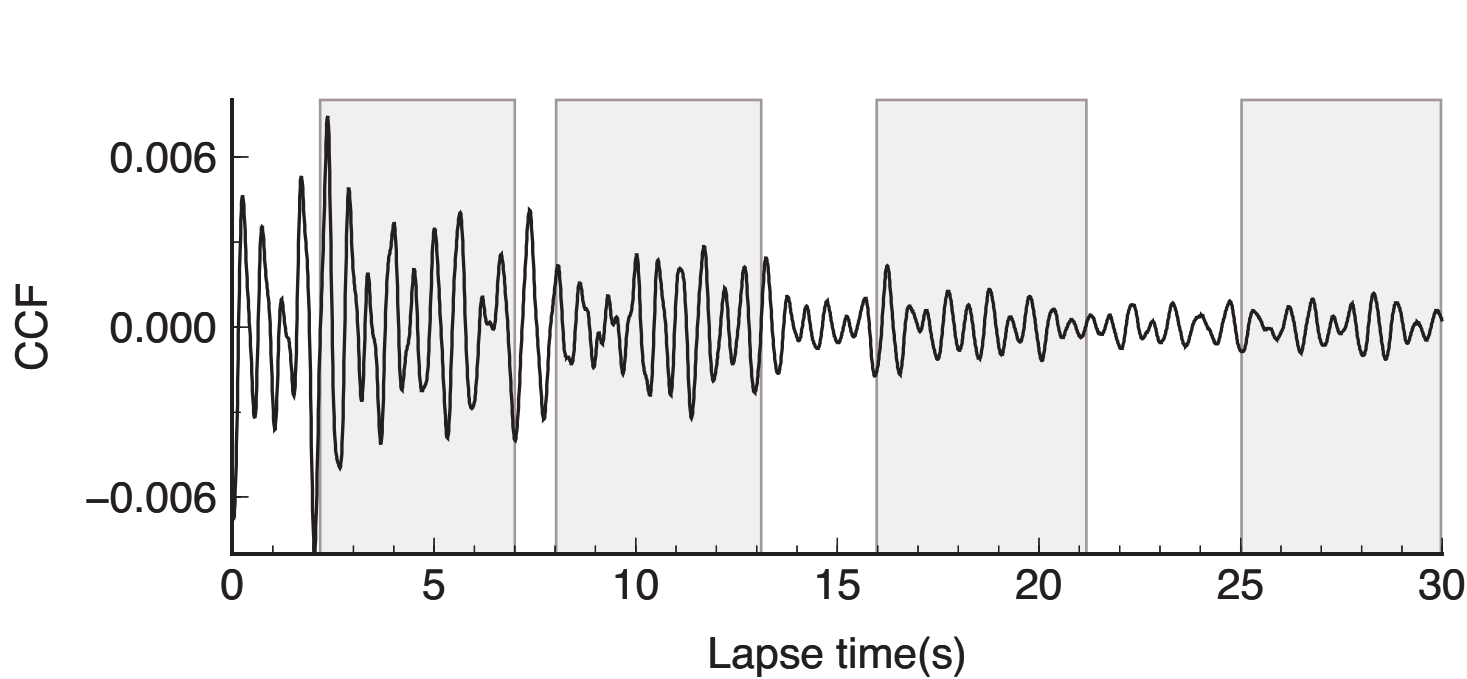
Accepted Article



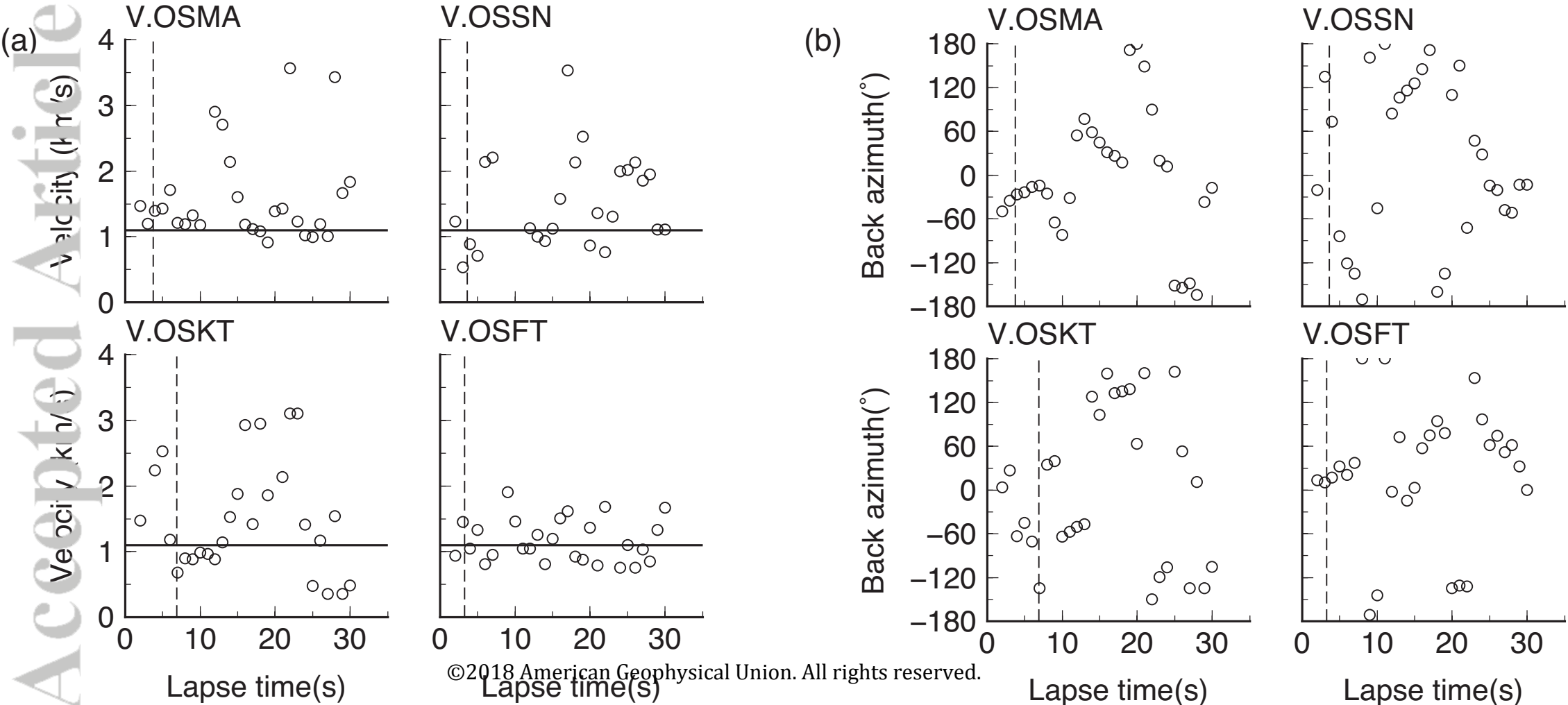
Accepted Article



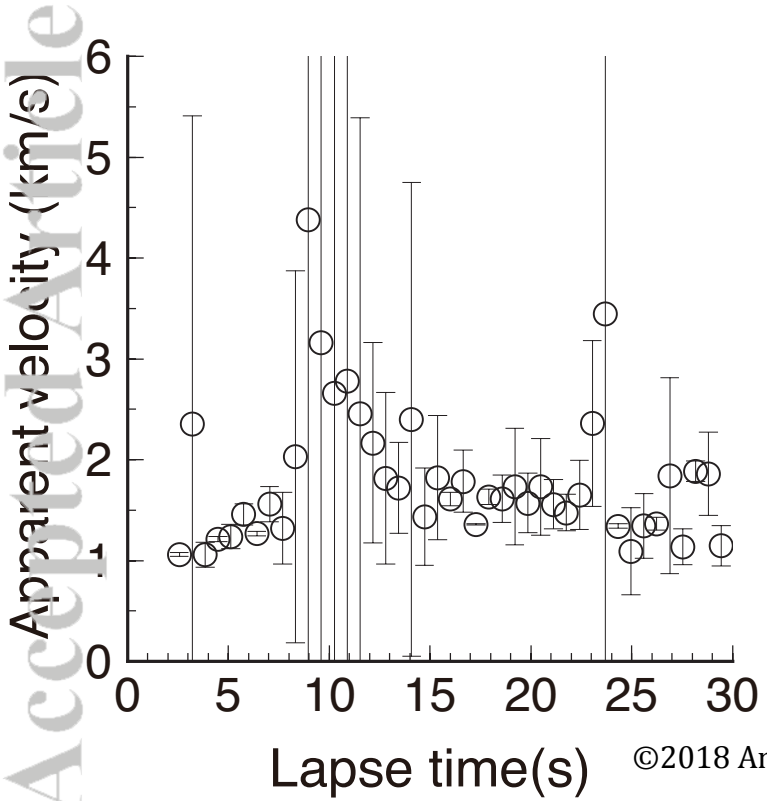
Accepted Article



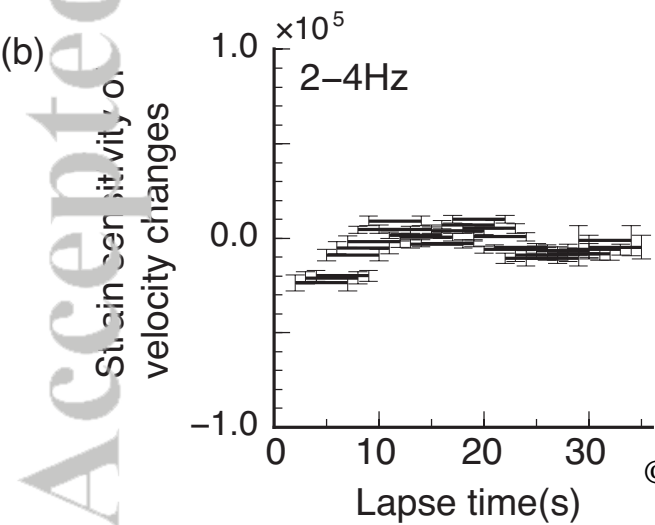
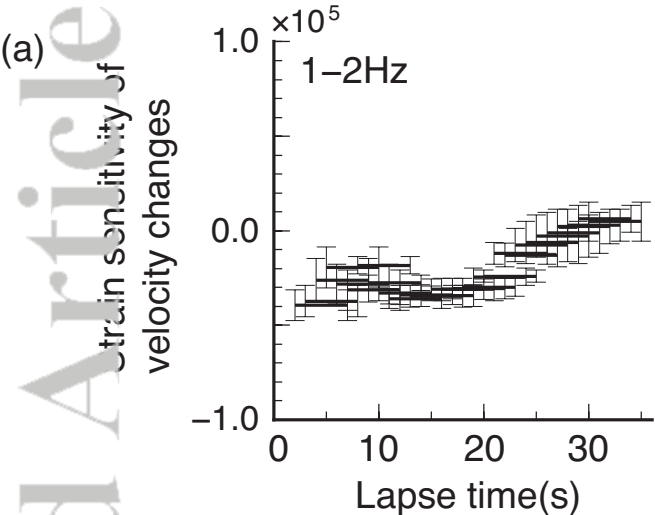
Accepted Article



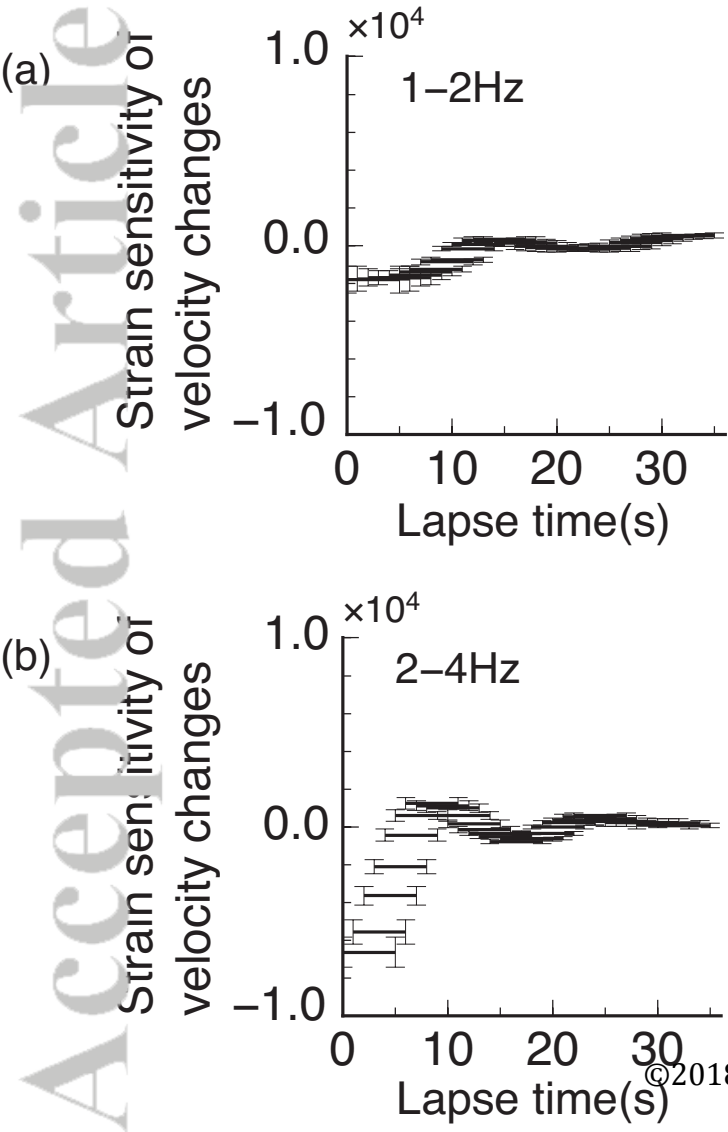
Accepted Article



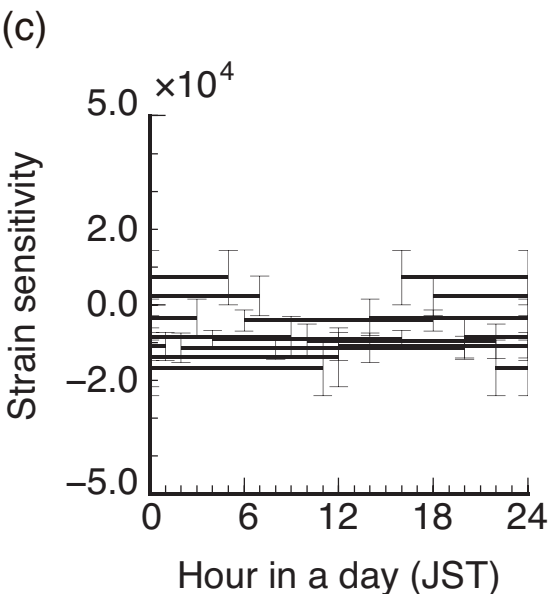
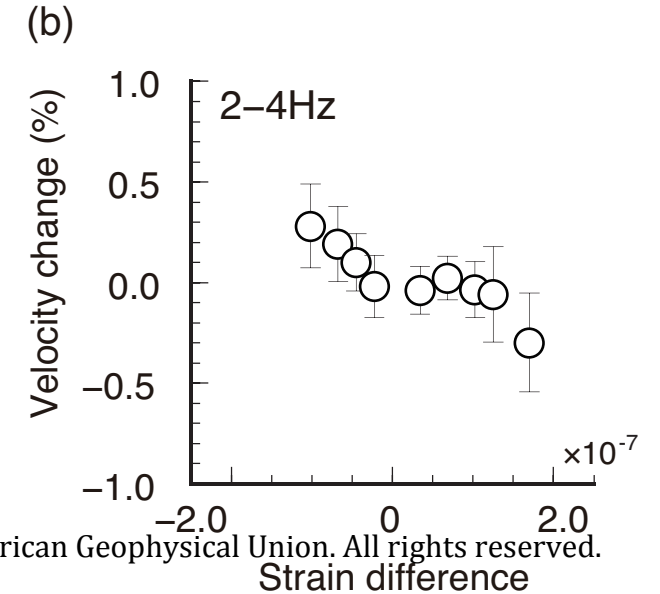
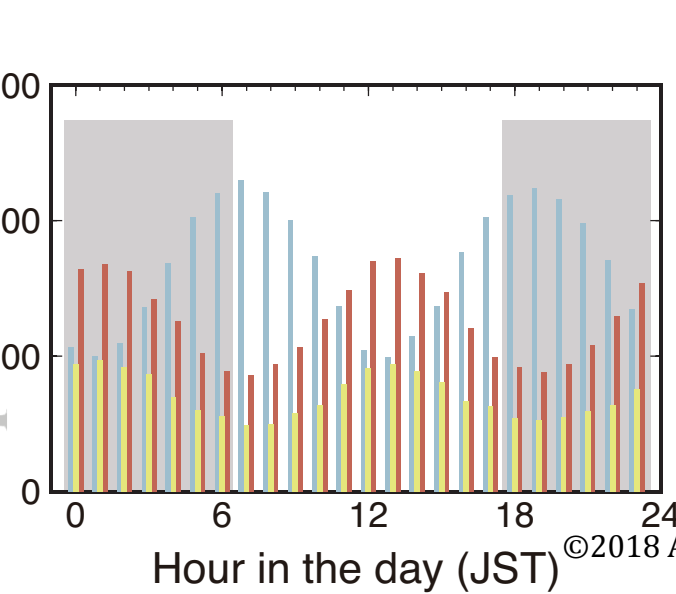
Accepted Article



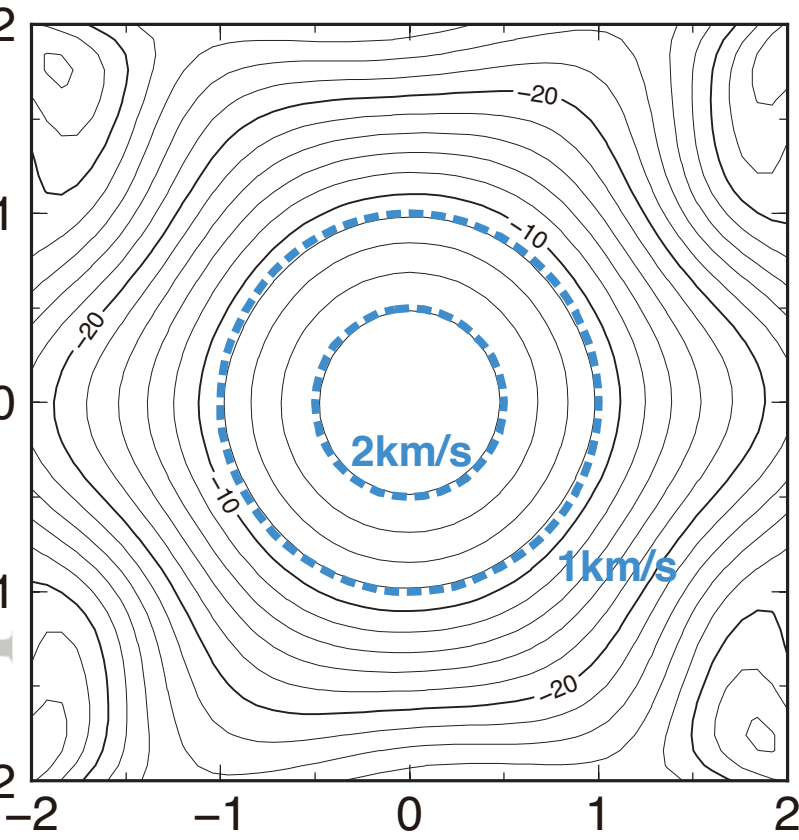
Accepted Article



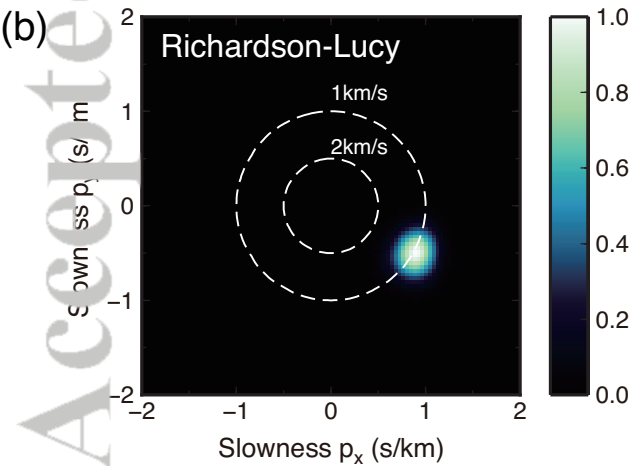
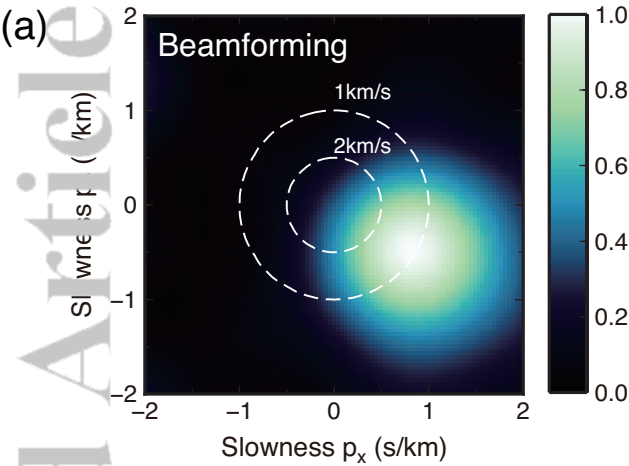
Accepted Article

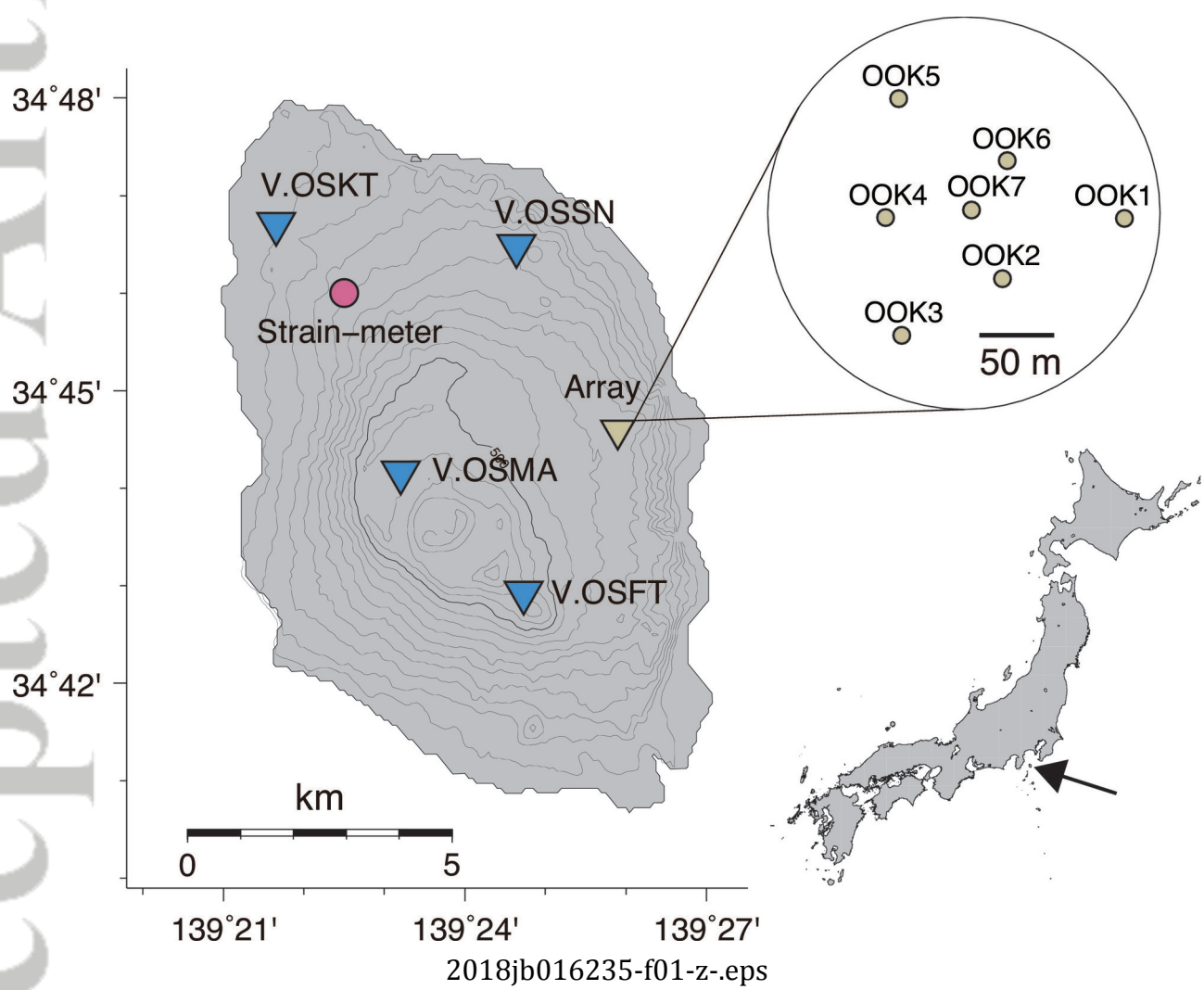


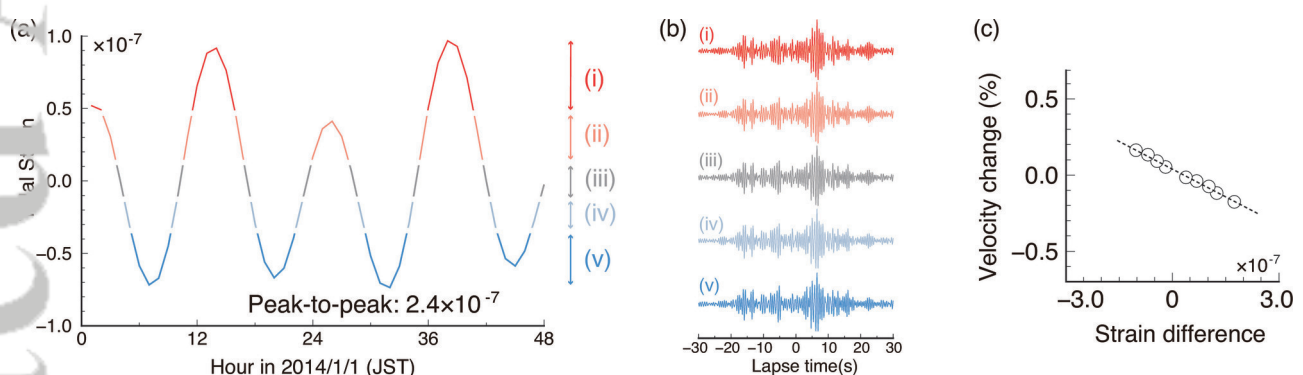
Accepted Article



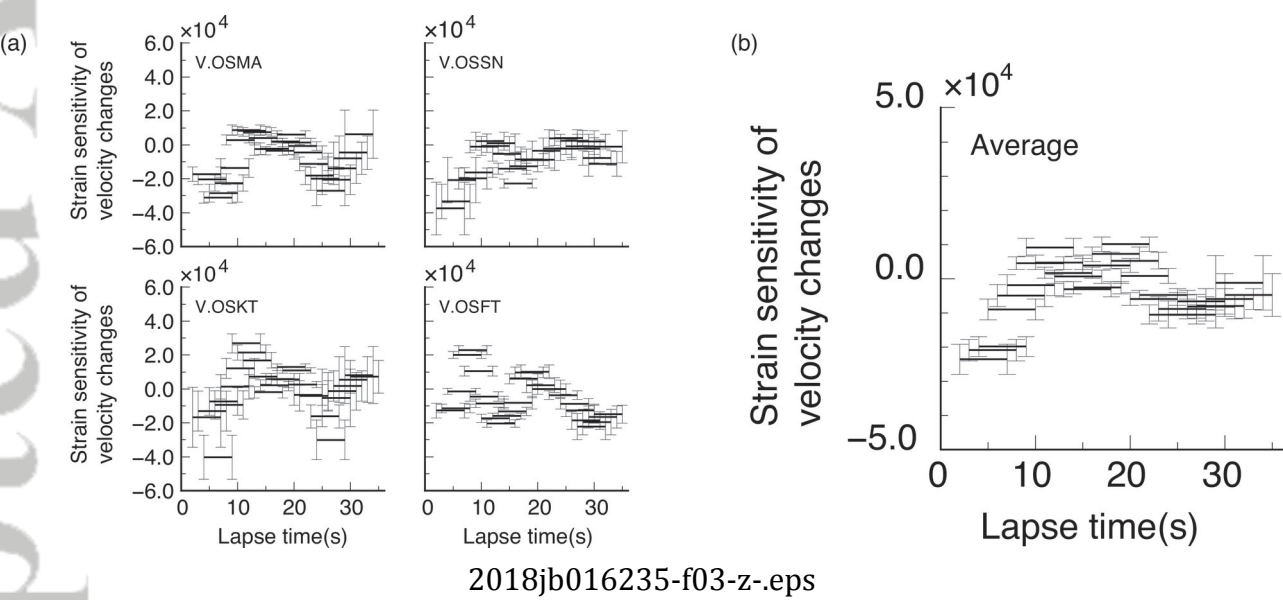
Accepted Article

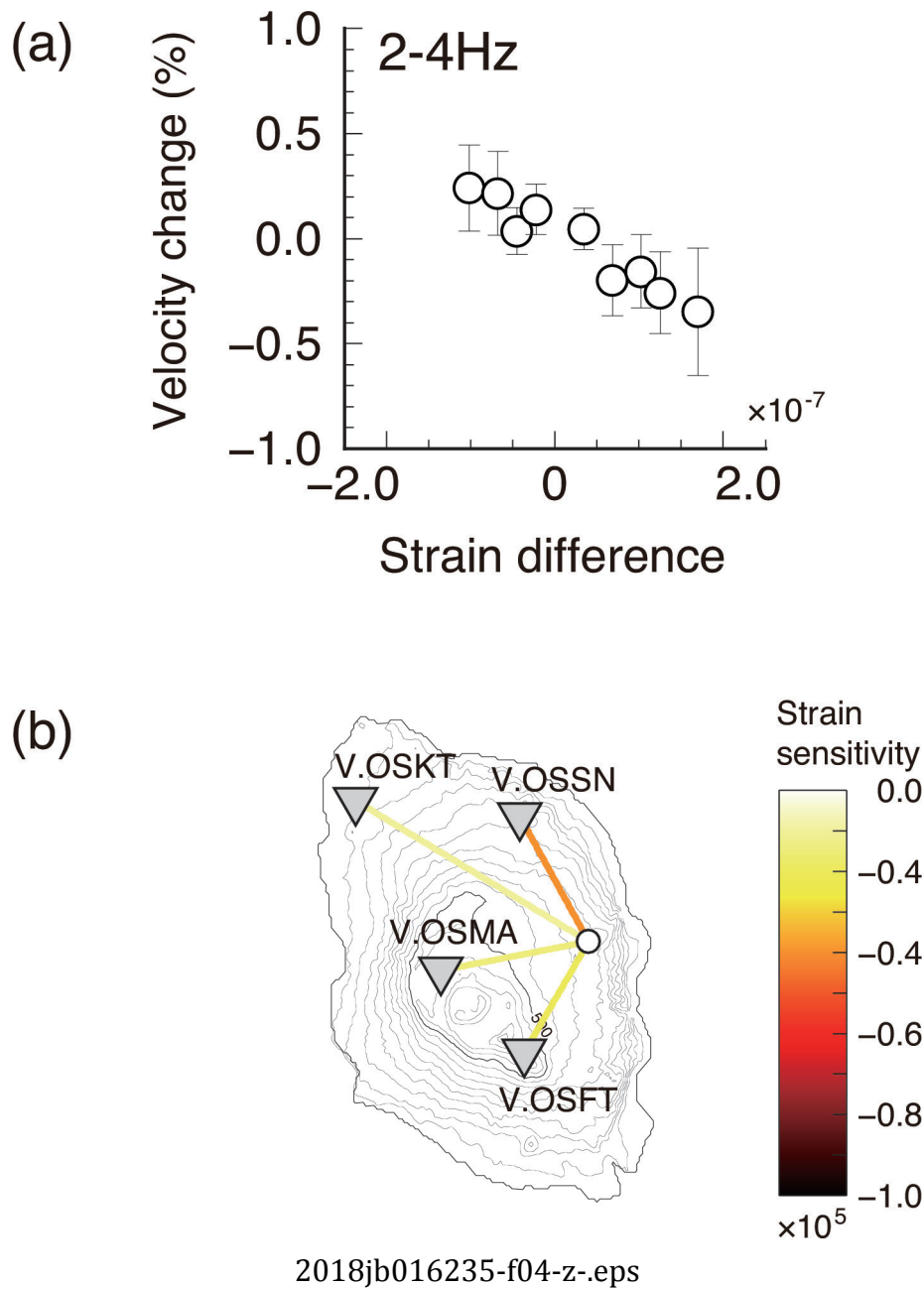




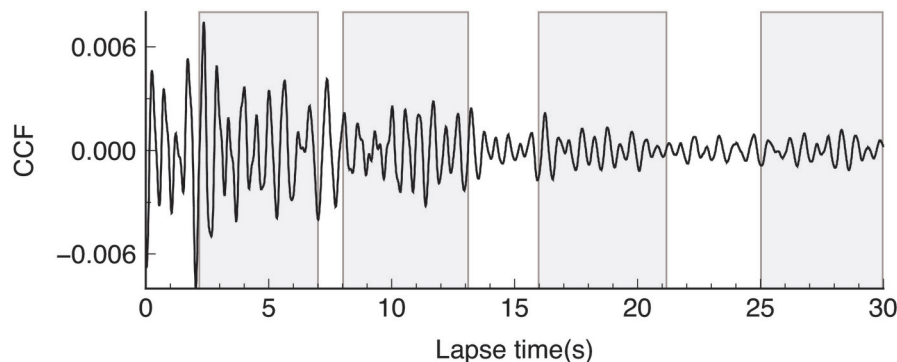


2018jb016235-f02-z-.eps

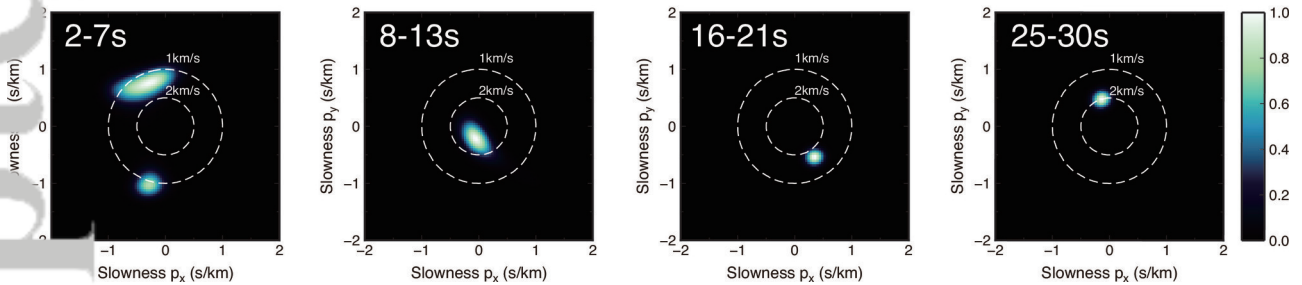




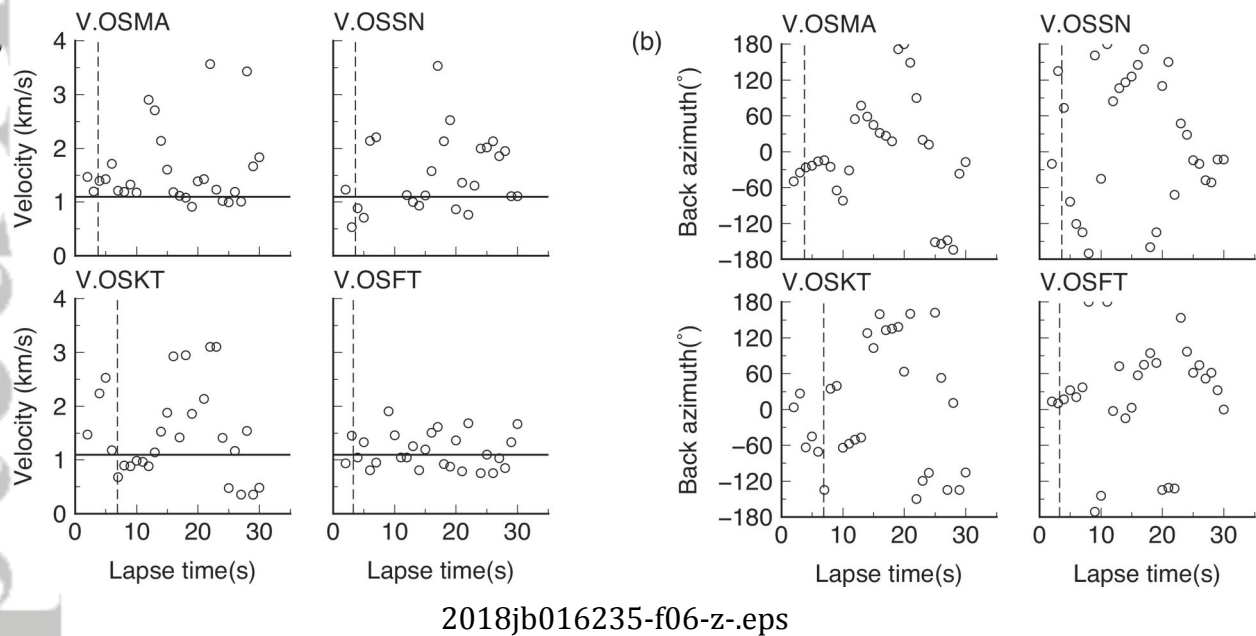
(a)

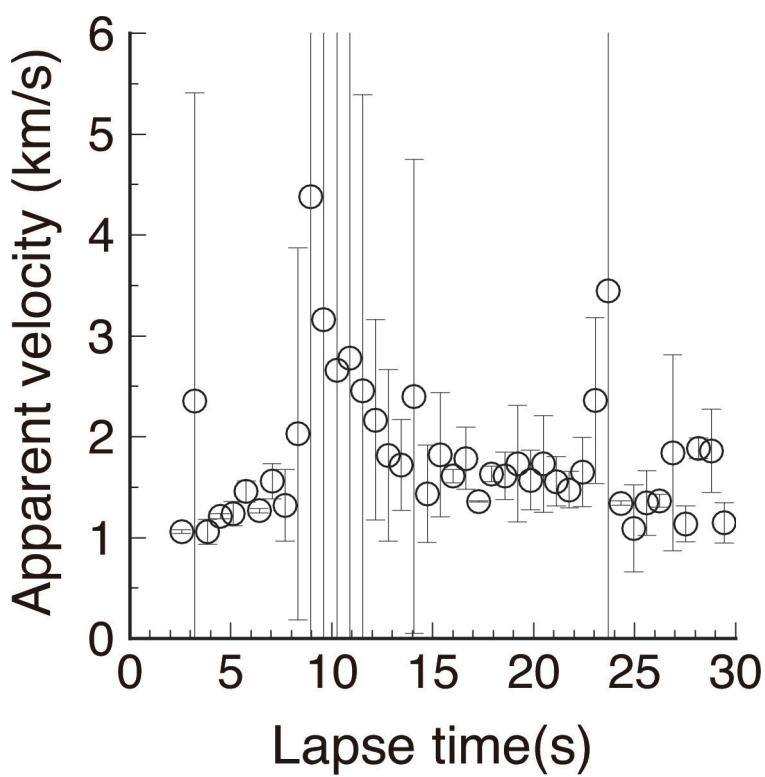


(b)

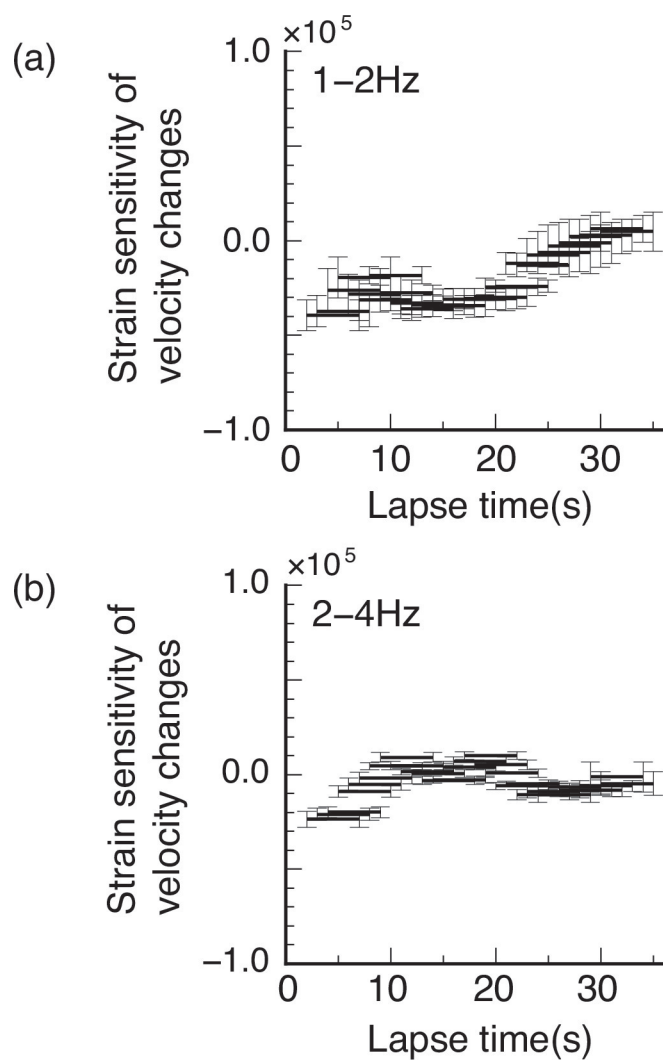


2018jb016235-f05-z-.eps

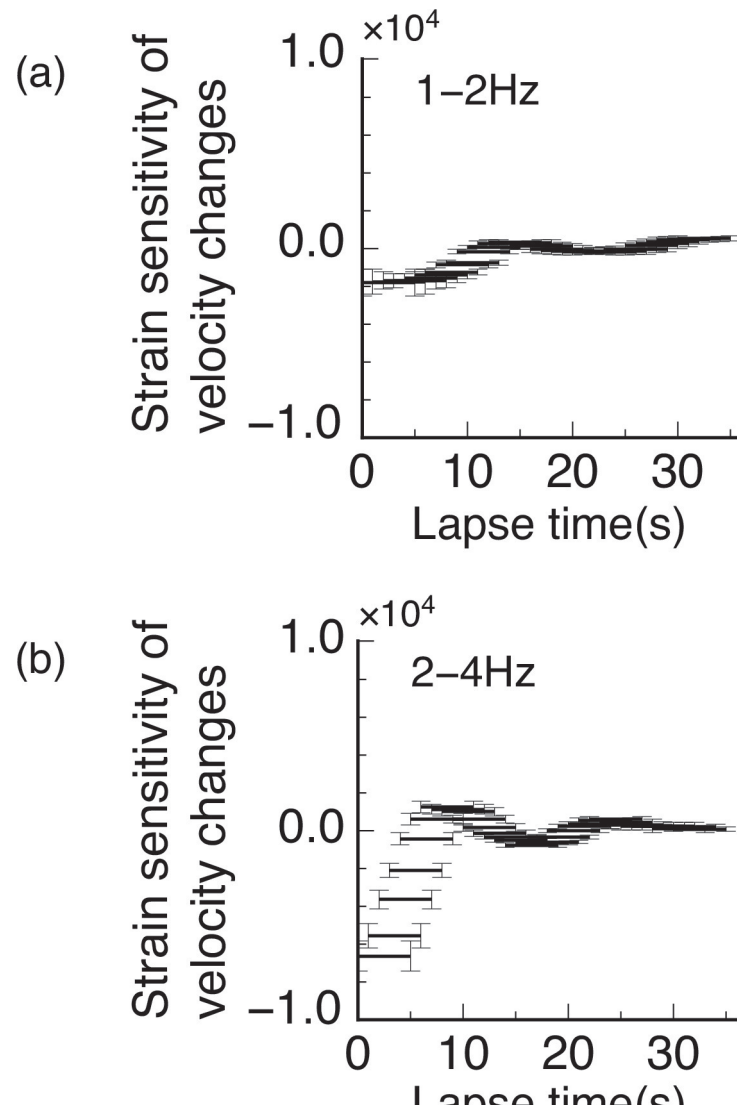




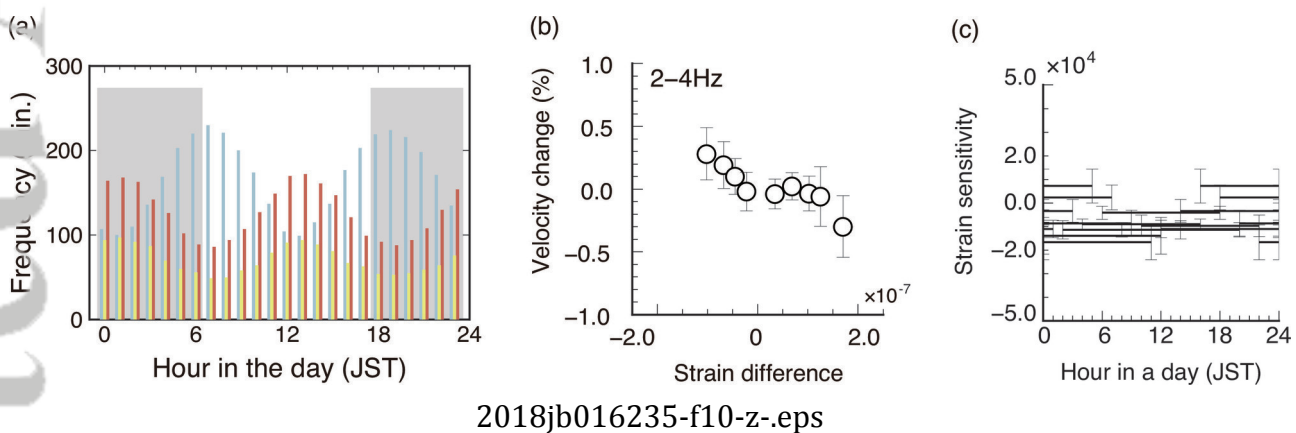
2018jb016235-f07-z-.eps

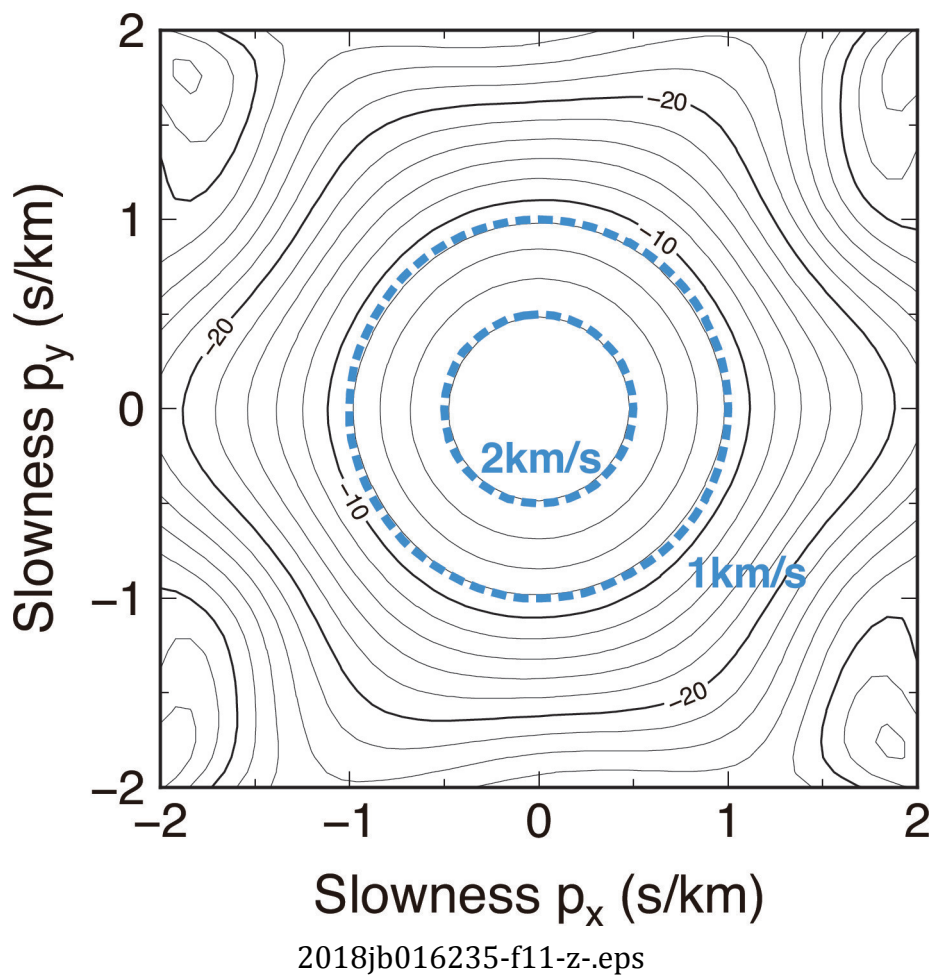


2018jb016235-f08-z.eps



2018jb016235-f09-z-.eps





2018jb016235-f11-z-.eps

